AGU PUBLICATIONS

Geochemistry, Geophysics, Geosystems

RESEARCH ARTICLE
10.1002/2015GC006016

Compositional variation and ^{226}Ra-^{230}Th model ages of axial lavas from the southern Mid-Atlantic Ridge, 8°48′S

K. M. Haase[1], P. A. Brandl[1,2], C. W. Devey[3], F. Hauff[3], B. Melchert[3], D. Garbe-Schönberg[4], T. F. Kokfelt[3,5], and H. Paulick[6,7]

[1]GeoZentrum Nordbayern, Friedrich-Alexander-Universität Erlangen-Nürnberg, Erlangen, Germany, [2]Now at Research School of Earth Sciences, Australian National University, Canberra, Australian Capital Territory, Australia, [3]GEOMAR Helmholtz-Zentrum für Ozeanforschung Kiel, Kiel, Germany, [4]Institut für Geowissenschaften, Christian-Albrechts-Universität, Kiel, Germany, [5]Now at The National Geological Survey of Denmark and Greenland, Copenhagen, Denmark, [6]Mineralogisches und Petrologisches Institut, Universität Bonn, Bonn, Germany, [7]Now at Boliden Mineral AB, Stockholm, Sweden

Key Points:
- Mid-Atlantic Ridge lavas show chemical variation on the scale of few km as well as with time
- Eruptions occur from axial volcanic ridges with repose periods of several 1000 years
- Volcanic units show variable degree of crystal fractionation and crustal contamination

Supporting Information:
- Supporting Information S1
- Table S1

Correspondence to:
K. M. Haase,
Karsten.Haase@fau.de

Citation:
Haase, K. M., P. A. Brandl, C. W. Devey, F. Hauff, B. Melchert, D. Garbe-Schönberg, T. F. Kokfelt, and H. Paulick (2016), Compositional variation and ^{226}Ra-^{230}Th model ages of axial lavas from the southern Mid-Atlantic Ridge, 8°48′S, *Geochem. Geophys. Geosyst.*, *17*, 199–218, doi:10.1002/2015GC006016.

Received 15 JUL 2015
Accepted 16 DEC 2015
Accepted article online 18 DEC 2015
Published online 29 JAN 2016

Abstract We present geological observations and geochemical data for the youngest volcanic features on the slow spreading Mid-Atlantic Ridge at 8°48′S that shows seismic evidence for a thickened crust and excess magma formation. Young lava flows with high sonar reflectivity cover about 14 km^2 in the axial rift and were probably erupted from two axial volcanic ridges each of about 3 km in length. Three different lava units occur along an about 11 km long portion of the ridge, and lavas from the northern axial volcanic ridge differ from those of the southern axial volcanic ridge and surrounding lava flows. Basalts from the axial rift flanks and from a pillow mound within the young flows are more incompatible element depleted than those from the young volcanic field. Lavas from this volcanic area have ^{226}Ra-^{230}Th disequilibria model ages of 1000 and 4000 years whereas the older lavas from the rift flank and the pillow mound, but also some of the lava field, are older than 8000 years. Glasses from the northern and southern ends of the southern lava unit indicate up to 100°C cooler magma temperatures than in the center and increased assimilation of hydrothermally altered material. The compositional heterogeneity on a scale of 3 km suggests small magma batches rising vertically from the mantle to the surface without significant lateral flow and mixing. The observations on the 8°48′S lava field support the model of low-frequency eruptions from single ascending magma batches that has been developed for slow spreading ridges.

1. Introduction

Lava eruptions along the mid-oceanic ridge system represent the volumetrically most important volcanic production on Earth [*Crisp*, 1984]. Typically, volcanic eruptions follow the ascent of magma through a dike and each of these events leads to growth of the oceanic crust [*Delaney et al*., 1998; *Sinton et al*., 2002]. Spreading rate appears to be an important factor in governing both magma chemistry and the relative importance of magmatic and tectonic processes for accommodating the plate separation. For example, at slow spreading axes, the lavas appear to be more primitive, melt lenses, when present, occur deeper, and mantle-inherited chemical variation appears to be larger indicating less efficient mixing processes [*Rubin et al*., 2009; *Sinton and Detrick*, 1992]. Closely related mid-ocean ridge lava flows, in some cases from one eruptive event, have been studied mainly on the East Pacific Rise, the Galapagos Spreading Center, and on Iceland where they have been shown to consist of lavas with variable compositions [*Colman et al*., 2012; *Hall and Sinton*, 1996; *Perfit and Chadwick*, 1998; *Sigmarsson et al*., 1991; *Sinton et al*., 2002; *Waters et al*., 2013]. In contrast, fewer studies exist on small-scale compositional variations of lavas on slow spreading ridges [*Sinton et al*., 2002; *Stakes et al*., 1984] and on the temporal evolution of volcanism at slow spreading ridges [*Rubin and Macdougall*, 1990; *Rubin et al*., 2009; *Sturm et al*., 2000]. The heterogeneity of melt inclusions within individual phenocrysts as well as the extreme compositional variation and zoning of minerals suggests mixing of highly variable magmas in the magmatic systems [e.g., *Dungan and Rhodes*, 1978; *Shimizu*, 1998]. Whereas some eruptions like that of Laki on Iceland produced lavas with relatively homogeneous compositions (Laki whole rock MgO range 5.64–5.88 wt %, K/Ti 0.21–0.22 [*Passmore et al*., 2012]), other lava flows show a significant chemical evolution during the eruption (e.g., Lambahraun, Iceland with a

range of MgO of 9.68–6.62 wt %, K/Ti 0.09–0.15 [*Eason and Sinton*, 2009]). Seismic tomographic and gravimetric studies of intermediate to slow spreading axes have revealed complex magma feeding systems beneath spreading segments, where different magma reservoirs appear to be laterally connected [*Canales et al*., 2006; *Magde et al*., 2000; *Peirce et al*., 2005]. Centers of slow spreading segments typically have shallower water depths and greater crustal thickness than the segment ends and this pattern is believed to reflect focusing of magma at the segment center [*Lin et al*., 1990; *Tolstoy et al*., 1993]. One model of the plumbing system suggests that magma ascends from the mantle preferentially in the center of a segment and flows then laterally toward the segment ends, either in the lower crust or through shallower dikes [*Abelson et al*., 2001; *Magde et al*., 2000]. Other authors suggest that melt is produced and ascends beneath the whole segment, at least at fast spreading segments and slow spreading segments with high magma production [*Tucholke et al*., 1997]. The ascending melt pools in sills at different depths in the crust [*Wanless and Shaw*, 2012] and in slow spreading segment centers, the lavas erupt periodically from axial volcanic ridges (AVR) above dike systems [*Head et al*., 1996; *Parson et al*., 1993; *Searle et al*., 2010; *Smith and Cann*, 1993]. An understanding of the chemical and petrologic composition, age, and size of single eruptive units can provide insights into the complex processes of magma generation and transport from the mantle to the surface.

Here we present observations and geochemical data on young eruptive units of the slow spreading southern Mid-Atlantic Ridge. Disequilibria of (^{226}Ra/^{230}Th) imply that most of the samples from the axial rift are younger than 8000 years, possibly in the range of 1000–4000 years. We find two ~3 km long axial volcanic ridges apparently fed by dikes erupting two lava units with significantly different incompatible element compositions. We conclude that along-axis magma transport is limited and individual dikes are fed by different magma batches from the mantle. Older lavas from the rift flank are more incompatible element depleted than those sampled in the rift axis and indicate significant changes of magma compositions with time.

2. Geological Setting

This study presents volcanologic and geochemical results on lavas from a relatively young lava field on the southern Mid-Atlantic Ridge (MAR) at about 8°48′S (Segment A2, Figure 1a) where the full spreading rate is about 33 mm/yr [*DeMets et al*., 1994]. Previous work divided the axis in this region into four second-order segments A1–A4 that are bounded by overlapping spreading centers [*Bruguier et al*., 2003]. The water depth decreases from about 3500 m on segment A1 to about 2500 m on segment A2 to only 1500 m on segment A3 (Figure 1a) before returning to 3500 m on segment A4. Seismic and gravimetric data indicate that crustal thickness also increases from 5 km on segment A1 to about 10 km in the center of segment A2 [*Bruguier et al*., 2003; *Minshull et al*., 1998]. Segment A2 does not show the deep axial rift typical of slow spreading axes but rather has a shallow axial rift valley and appears to be magmatically inflated [*Bruguier et al*., 2003]. Geochemical and geophysical data suggest that a melting anomaly underlies segments A2 and A3 because these two segments are unusually shallow, have a thickened crust of 10–11 km, and erupt lavas with incompatible element-enriched and radiogenic Sr and Pb isotopic composition [*Hanan et al*., 1986; *Hoernle et al*., 2011; *Minshull et al*., 1998]. The occurrence of three off-axis seamounts near 9°40′S is further evidence for excess magma formation in this region, with the immediately adjacent area of the spreading axis showing the shallowest depths (Figure 1a) and erupting the most incompatible-element-enriched lavas [*Hoernle et al*., 2011]. The recent studies prefer an origin of the melting anomaly by passive entrainment of enriched upper mantle portions rather than an influence by enriched and excessively hot deep mantle plume material [*Hoernle et al*., 2011; *Minshull et al*., 1998]. The bathymetric and magnetic data suggest that segment A2 is propagating northward into the deeper A1 segment [*Brozena and White*, 1990; *Bruguier et al*., 2003].

3. Sampling and Analytical Methods

3.1. Sampling and Observations

During Meteor cruise M62/5 in November 2004, the southern MAR was mapped using the TOBI side scan system [*Devey et al*., 2005]. A large area of high and homogeneous reflectivity was observed between about 8°46′S and 8°50′S in the MAR rift close to the center of segment A2 (Figure 1c). Numerous volcanic structures are visible on the side scan image suggesting that the highly reflective area represents an extensive

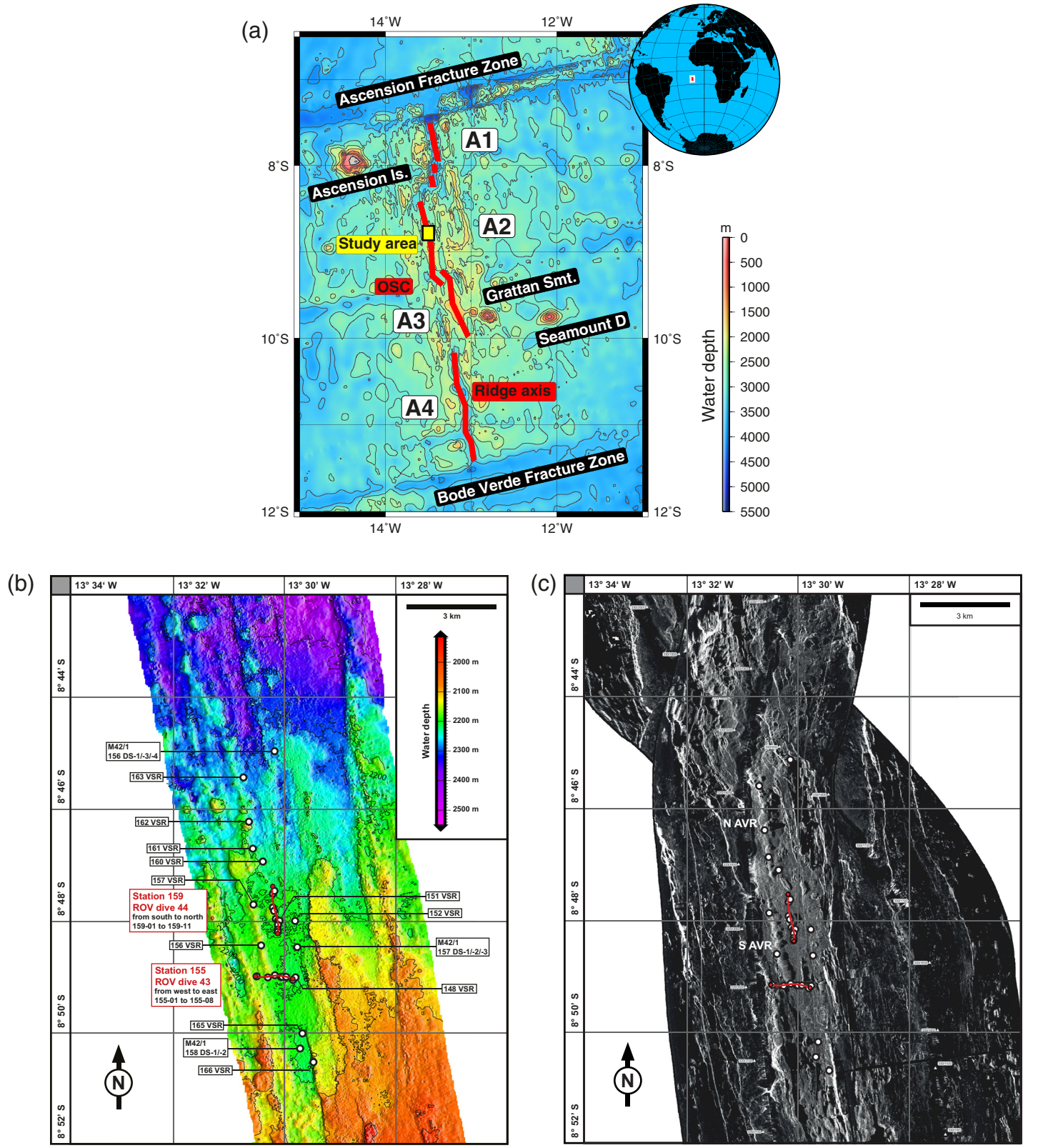

Figure 1. (a) Overview of the segments of the southern Mid-Atlantic Ridge. The study area is in the center of the segment A2 that is propagating northward. (b) Bathymetric map of the lava field in segment A2 showing the sample sites of the ROV dives, the rock corer (VSR), and dredges (DS) as circles. The red lines show the two ROV tracks where the southern track is 155ROV across and the northern is 159ROV along the rift. (c) TOBI side-scan sonar map of the volcanic field at 8°48′S on the southern MAR. The ROV dive tracks and the sampling stations are shown as in Figure 1b.

field of relatively recent volcanic activity. An earlier cruise M42/1 to the southern MAR retrieved three dredges (156, 157, and 158 DS) in the area, but the A2 volcanic field was first sampled in detail during the Meteor 64/1 cruise in April 2005 with two dives with the MARUM QUEST4000 ROV and 12 wax corer (VSR) stations (Figure 1b). The ROV was navigated using a self-calibrating acoustic IXSEA GAPS USBL positioning system allowing positioning accurate to within ~1% of water depth (±23 m at the depths considered here). Lava samples were taken with the hydraulic arms of the ROV. Some 30 new samples containing fresh volcanic glass were recovered from 20 stations including two ROV transects across and along the field (Figure 1b).

3.2. Geochemical Analyses of Glasses and Minerals

The glass was separated from the samples by hand picking and cleaned using deionized water in an ultrasonic bath. Glass chips were polished and analyzed for their major element composition on a JEOL Superprobe electron microprobe at the University of Kiel using standard wavelength-dispersive techniques. The instrument was operated at an accelerating voltage of 15 kV and beam currents of 20 nA. The beam diameter during calibration and sample measurement was 12 μm. Counting times on peaks and background varied depending on the element analyzed, and were 20 s for all major elements except Na_2O which was analyzed with peak counting times of 10 s. Background counting times were always half of peak counting times. Individual glass chips were analyzed 10 times at different parts and the average was calculated. Data for major elements as well as S and Cl contents of the glasses are shown in the supporting information table together with data for the VG-2 glass standard run with the samples. Mineral compositions were determined on polished thin sections on the same electron microprobe but with a focused beam.

Representative glass samples were analyzed for trace elements by ICP-MS following the general procedure described previously [*Garbe-Schönberg*, 1993] but now using an Agilent 7500cs instrument and these data were published previously [*Hoernle et al*., 2011]. About 50 mg of glass chips were washed repeatedly with MQ water in an ultrasonic bath and were then dissolved in a hot HF-HNO_3 mixture and dried until they could be completely digested in a 10% HNO_3 solution. Accuracy is evaluated from within-batch analyses of international rock standards (BIR-1 and BHVO-1, supporting information table). The results for BIR-1 and BHVO-1 are within 10% for most elements of recommended values [*Govindaraju*, 1994; *Jochum et al*., 1990], and usually better than 3% for REE. The instrumental reproducibility of repeated analysis of samples is generally better than 1.0% for all elements.

The Sr, Nd, and Pb isotope data are from *Hoernle et al*. [2011] and U series isotope data are from *Turner et al*. [2015]. Sr-Nd-Pb isotope analyses (Table 1) were carried out on fresh glass chips (100–250 mg) that were leached in warm 2 N HCl (70°C, 1 h) and subsequently rinsed three times in ELGA water. The leached chips were dissolved for 2 days in a 5:1 mixture of ultrapure HF and HNO_3 at 150°C and ion exchange procedures followed established standard procedures. Isotope analyses were carried out in static multicollection mode on Finnigan MAT 262 RPQ2+ (Pb) and Thermo Finnigan TRITON-TI (Sr, Nd) thermal ionization mass spectrometers (TIMS). Sr and Nd isotopic ratios were normalized within run to $^{86}Sr/^{88}Sr = 0.1194$ and $^{146}Nd/^{144}Nd = 0.7219$, respectively, and all errors are reported as 2 sigma of the mean. Standards measured along with the samples were normalized for each batch and gave $^{87}Sr/^{86}Sr = 0.710250 \pm 0.000008$ (n = 53) for NBS987 and $^{143}Nd/^{144}Nd = 0.511850 \pm 0.000006$ (n = 42) for the La Jolla Nd standard. Pb isotope ratios were determined using the Pb double-spike (Pb-DS) technique. Using the SBL74 spike, the double spike corrected NBS981 values measured along with the samples are $^{206}Pb/^{204}Pb = 16.9416 \pm 0.0024$, $^{207}Pb/^{204}Pb = 15.4998 \pm 0.0024$, $^{208}Pb/^{204}Pb = 36.7231 \pm 0.0063$, $^{207}Pb/^{206}Pb = 0.91490 \pm 0.00005$, and $^{208}Pb/^{206}Pb = 2.16763 \pm 0.00013$ (n = 30). Total Pb chemistry blanks were 20–40 pg and thus are considered negligible. For the U series isotope analyses, we used millimeter-sized clean glass chips that were separated under a binocular microscope. Between 0.2 and 0.7 g of glass were leached for 10 min with a 1:1 mixture of 2.5 *M* HCl and 30% hydrogen peroxide in an ultrasonic bath at room temperature and then rinsed several times in Milli-Q water. The U-Th-Ra isotope ratios were determined by TIMS at GEOMAR, Kiel following the methods outlined in *Kokfelt et al*. [2005]. The Th measurements were determined by the ^{229}Th-bridge technique whereby the $^{230}Th/^{232}Th$ ratio is acquired in two dynamic steps on the RPQ-SEM. Internal analytical errors are presented in the supporting information table as well as results for multiple (n = 6) analyses of the Table Mountain Latite (TML) rock standard.

Table 1. Location and Description of the Samples From the Area of the Young Volcanic Area at 8°48′S on the Mid-Atlantic Ridge[a]

Cruise Sample	Volcanic Structure	Latitude °S	Longitude °W	Water Depth (m)	Sample Description
M64/1 159ROV-6	Old lava, pillow mound in axis	8°47.81′	13°30.19′	2151	Pillow lava, abundant fragments of aphyric basalt glass shards
M64/1 159ROV-5	Old lava, pillow mound in axis	8°47.96′	13°30.16′	2186	Pillow lava, piece of lava protrusion, plag-phyric glassy basalt, 10 vol % plag ph to 10 mm, surface with striation marks, glass crust partially palagonitized and covered by thin layer of black Mn-oxide Phyric, hypocrystalline, fine-grained, intersertal, less vesicles, >80% matrix, >10% plag (microlites and zoned ph), <10% cpx ph with Cr-spl inclusions
M41/2 156DS-1	Old lava from rift flank	8°44.96′ 8°45.01′	13°30.18′ 13°29.80′	2257–2255	Pillow lava with 1 mm glass rim, plag ph to 6 mm, Mn coating
M41/2 156DS-3	Old lava from rift flank	8°44.96′ 8°45.01′	13°30.18′ 13°29.80′	2257–2255	Pillow lava with 6 mm glass rim, plag ph to 8 mm, ol ph to 1 mm, vesicles to 2 mm diameter
M41/2 156DS-4	Old lava from rift flank	8°44.96′ 8°45.01′	13°30.18′ 13°29.80′	2257–2255	Pillow tube with 3 mm glass rim, few vesicles to 2 mm diameter
M64/1 155ROV-1	Old lava from rift flank	8°48.98′	13°30.50′	2161	Pillow lava, glassy basalt from talus breccia, covered by mud, rare <1 mm ol ph
M64/1 148VSR	Old lava from rift flank	8°49.00′	13°29.80′	2230	Small chips of gray, microcrystalline aphyric basalt, trace of glass chips
M64/1 159ROV-10	Southern smooth volcanic area	8°47.46′	13°30.18′	2219	Sheet flow, small lava fold with glassy crust (1–2 mm), plag-phyric basalt, 1% plag up to 1 mm
M64/1 159ROV-11	Southern smooth volcanic area	8°47.46′	13°30.18′	2219	Sheet flow, lava lobe of 4 cm thickness with glassy crust on both sides, abundant palagonitization, 1% plag ph to 5 mm, rare ol. Phyric, hypocrystalline, spherulitic, ~80% fresh glass, >10% plag ph (partly zoned), ~5% cpx ph
M64/1 159ROV-9	Southern smooth volcanic area	8°47.50′	13°30.21′	2215	Pillow lava, top is glassy (1–2 mm thick), slight palagonitization, <1% plag and ol, up to 1 mm, lower surface is undulated, solidified lava droplets
M64/1 159ROV-7	Southern smooth volcanic area	8°47.75′	13°30.21′	2201	Pillow lava, plag-phyric basalt with 2 mm glass crust, <1% ph plag ph to 1 mm, 3% vesicles to 2 mm, several zones of shearing up to 10 mm wide oriented parallel to the surface spaced at 2–4 cm intervals. Slight Fe-Oxihydroxide staining. Phyric, hypocrystalline, ~70% matrix with spherulitic plag microlites (~15% in total), ~10% vesicles, <5% ol ph with Cr-spl inclusions
M64/1 159ROV-8	Southern smooth volcanic area	8°47.76′	13°30.21′	2202	Sheet flow, basalt with 1–2 mm glass crust, slightly palagonitized, few plag ph (<1 mm), 1 vol % vesicles up to 1 mm
M64/1 152VSR	Southern smooth volcanic area	8°47.99′	13°29.81′	2223	Several glass pieces
M64/1 151VSR	Southern smooth volcanic area	8°47.99′	13°30.10′	2219	Basalt glass
M64/1 159ROV-4	Southern smooth volcanic area	8°47.99′	13°30.12′	2201	Sheet flow, aphyric glassy basalt, abundant shards <1–3 cm in foram./pteropod sand
M64/1 159ROV-3	Southern smooth volcanic area	8°48.06′	13°30.12′	2198	Jumbled flow, aphyric glassy basalt; flow fold quenched on both sides, slight palagonitization, microcrystalline groundmass surrounds elongate cavity (long axis > 4 cm parallel to fold axis)
M64/1 159ROV-2	Southern smooth volcanic area	8°48.15′	13°30.12′	2201	Sheet flow, basalt with 3 mm glass crust, <1% plag ph, 2% vesicles up to 2 mm, minor Fe staining
M64/1 159ROV-1	Southern smooth volcanic area	8°48.18′	13°30.12′	2204	Pillow lava, glassy basalt with 1% ol and plag ph up to 1 mm, some palagonite
M41/2 157DS-1	Southern smooth volcanic area	8°48.46′ 8°48.78′	13°29.77′ 13°29.41′	2212–2079	Sheet flow, few vesicles, 15 mm glass rim, aphyric
M41/2 157DS-2	Southern smooth volcanic area	8°48.46′ 8°48.78′	13°29.77′ 13°29.41′	2212–2079	Sheet flow, few vesicles, slightly altered glass rim, aphyric
M41/2 157DS-3	Southern smooth volcanic area	8°48.46′ 8°48.78′	13°29.77′ 13°29.41′	2212–2079	Sheet flow, few vesicles, 15 mm glass rim, aphyric, vesicular
M64/1 155ROV-4	Southern smooth volcanic area	8°48.96′	13°30.17′	2195	Pillow lava, aphyric basalt, pillow section, microcrystalline with partially palagonitized glass crust (~1 mm); 2% vesicles up to 2 mm
M64/1 155ROV-7	Southern smooth volcanic area	8°48.99′	13°29.97′	2221	Abundant aphyric basalt glass chips of pillow lava crust. Partially palagonitized
M64/1 155ROV-5	Southern smooth volcanic area	8°48.99′	13°30.06′	2199	Pillow lava, altered aphyric basalt with <1% cpx and rare plag (<1 mm). Piece consists of two individual lobes showing ductile deformation
M64/1 155ROV-6	Southern smooth volcanic area	8°48.99′	13°30.04′	2190	Piece of pillow lava crust with prominent striated top surface texture. Roof (3 cm thick) of partially drained pillow. Glass

Table 1. (continued)

Cruise Sample	Volcanic Structure	Latitude °S	Longitude °W	Water Depth (m)	Sample Description
					on both sides (top: 2–4 mm; base < 1 mm). Partial palagonitization. 1% ol ph up to 5 mm
M64/1 155ROV-8	Southern smooth volcanic area	8°49.04′	13°29.85	2218	Pillow lava, single piece of microcrystalline basalt with 1% ol ph (up to 1 mm); ~1% vesicles (up to 2 mm). Glass crust is 1–3 mm thick and locally shows spherulitic textures.
M64/1 165VSR	Southern smooth volcanic area	8°50.00′	13°29.68′	2225	Aphyric basalt glass
M41/2 158 DS-1	Southern smooth volcanic area	8°51.27′ 8°51.59′	13°29.72′ 13°29.00′	2139–2086	Sheet flow, fresh 10 mm thick glass rim, aphyric, vesicles to 2 mm
M41/2 158 DS-2	Southern smooth volcanic area	8°51.27′ 8°51.59′	13°29.72′ 13°29.00′	2139–2086	Pillow lava, less fresh than −1, glass less than 2 mm thick, aphyric, few vesicles
M64/1 166VSR	Southern smooth volcanic area	8°50.51′	13°29.48′	2188	Chips and fragments of microcrystalline and glassy basalt.
M64/1 155ROV-3	Southern axial volcanic ridge	8°49.00′	13°30.30′	2149	Lobate flow, 4 cm thick roof of lava lobe. Top surface is glassy (2 mm thick), 5% vesicles up to 5 mm in the microcrystalline basalt below the glass crust; lower surface with stalagtite texture; rare ol ph < 1 mm
M64/1 156VSR	Southern axial volcanic ridge	8°48.43′	13°30.42′	2208	Basalt glass
M64/1 157VSR	Southern axial volcanic ridge	8°47.70′	13°30.56′	2190	Basalt glass
M64/1 160VSR	Northern axial volcanic ridge	8°46.93′	13°30.39′	2208	Basalt glass
M64/1 161VSR	Northern axial volcanic ridge	8°46.70′	13°30.57′	2266	Basalt glass with plagioclase phenocrysts
M64/1 162VSR	Northern axial volcanic ridge	8°46.22′	13°30.64′	2273	Basalt glass with plagioclase phenocrysts
M64/1 163VSR	Northern axial volcanic ridge	8°45.43′	13°30.74′	2287	Basalt glass with plagioclase phenocrysts

[a]ROV, sample taken with remotely operated vehicle (ROV); DS, dredge sample (start and end points given); VSR, rock corer, ph, phenocrysts; ol, olivine; cpx, clinopyroxene; plag, plagioclase; Cr-spl, Cr-spinel; Mn, manganese; Fe, iron.

4. Results

4.1. Geological Observations on the Volcanic Field

The young volcanic area shown in Figure 1c covers about 14 km^2 within the 1.5–2 km wide axial rift valley and occurs north of the segment A2 center. The volcanic area on the rift floor is about 8 km long and has a maximum width of 2 km. The rift valley itself is bounded by normal faults that were identified as very high reflectivity, linear features on the TOBI images (Figure 1c). The rift floor in this region deepens from about 2200 m water depth in the south to 2300 m water depth in the north. The deployment of autonomous turbidity loggers (MAPRs) [*Baker and Milburn*, 1997] at 15 rock corer and CTD stations in the region between 8°48′S and 8°50′S showed no indication of a hydrothermal particulate plume in the water column. No hydrothermal activity was observed during the two ROV dives in this area. Although the young volcanic area frequently abuts faults at the rift flanks, the high backscatter area itself shows relatively few and small faults. Within the area of the volcanic fields, two rows of small volcanic cones form a southern and a northern axial volcanic ridge (AVR) [*Head et al*., 1996; *Smith and Cann*, 1993] with heights up to about 50 m and about 3 km length each (Figure 1). An interpretation of the TOBI image in terms of major volcanic and tectonic structures is shown in Figure 2 and we follow the descriptions of *Smith and Cann* [1993] with hummocks referring to mounds with variable diameters whereas smooth areas do not show distinct structures in the side scan images. The area directly surrounding these two AVRs has a hummocky surface (shown as "Hummocky 1" on Figure 2) compared to the smoother area ("Smooth 1") more distant from the cones. At about 8°48′S, a volcanic mound ("Pillow Mound" on Figure 2) with a diameter of about 400 m and a height of about 50 m was imaged east of the southern AVR within the Smooth 1 volcanic region (Figures 1c and 2). The relatively smooth, high backscatter area in the axial rift contrasts with the low reflectivity, abundant large faults, and very rough terrain seen on the rift flanks ("Hummocky" 2 and 3 and "Smooth" 2, 3, and 4 on Figure 2). Observations by ROV show that fault surfaces are typically steep and have heights of up to 30 m. Both sides of the volcanic field are bounded by normal faults and camera observations indicate that these mark the transition from older sediment-covered flank lavas to the lavas with little sediment cover in the axial rift.

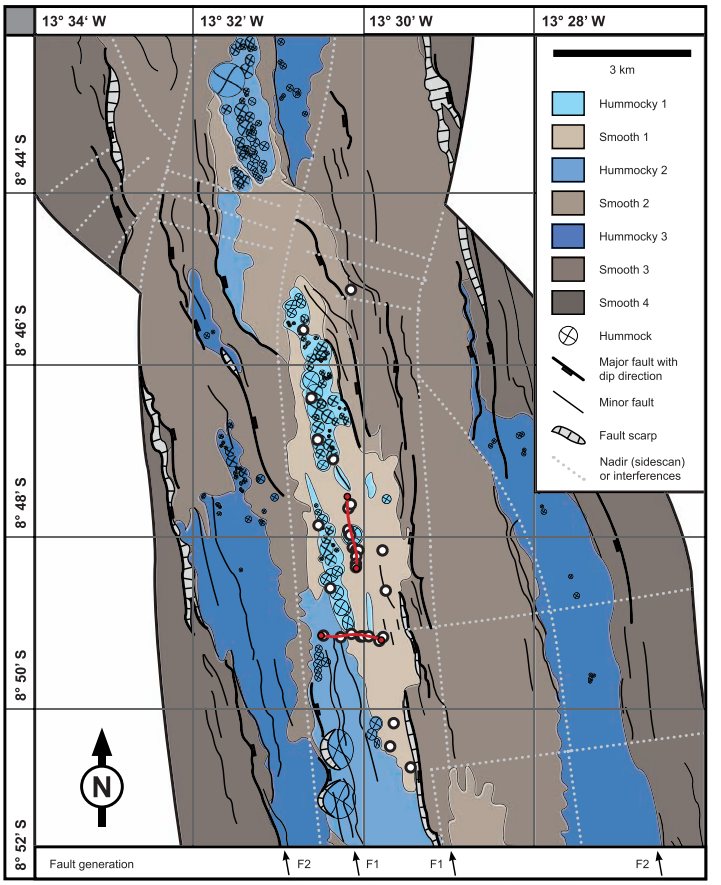

Figure 2. Map with the interpretation of tectonic and volcanic structures based on the bathymetric data and TOBI side scan observations of the volcanic field at 8°48′S. The description of smooth and hummocky terrains is done following *Smith and Cann* [1993]. The Hummocky 1 and Smooth 1 areas have the highest reflectivity and are probably the youngest areas in Figure 1c. Most samples are from these units.

Our study with two ROV dives concentrated on the Hummocky 1 and the surrounding Smooth 1 region that forms the youngest volcanic area in this segment of the MAR. To study the transition from the Hummocky 2 to the Hummocky 1/Smooth 1 regions, we started dive 155ROV on the western rift flank (Figure 2). The 155ROV dive led from the western rift flank across the southern end of the southern AVR (Figures 1b, 1c, and 2) and is illustrated in Figure 3a. Several large normal fault scarps with throws of 5–20 m and abundant talus piles were traversed in the Hummocky 2 region of the rift flank. The lavas on the western rift flank are mainly pillows and lobate flows that are heavily faulted and sedimented (Figure 3a, photos a and b). In contrast, the acoustically highly reflective and smooth rift center consists of lobate and pillow lavas with little faulting and sediment generally occurring in patches (Figure 3a, photos c–h). Close to the southern SVR, the faults are typically 0.5–1 m wide without large offsets (Figure 3a, photo f). Lava morphology in the rift axis is dominated by pillow and lobate flows but sheet and jumbled sheet flows with collapse structures also occur (Figure 4). Several contacts of younger lava above an older lava formation were observed (Figures 4e and 4f). The ~30 m high volcanic edifice of the southern AVR also consists of lobate and pillow lavas and shows sheet flows and collapse pits on the top (Figure 3a, photo c). Further east on the relatively flat rift floor, we observed again pillow and lobate lavas with evidence of some faulting and numerous volcanic fissures with collapse pits. Collapse pits have diameters up to 20 m and depths of about 5 m (Figure 4d). The eastern part of the Smooth 1 area shows more sediment on the lavas and abundant west-facing normal faults with throws of 10–20 m (Figure 3a, photos f–h). During this dive, we recovered two samples (155ROV-1 and 155ROV-2) from the western rift flank lavas, one (155ROV-3) from the southern end of the southern AVR and five samples (155ROV-4 to 155ROV-8) were taken on the Smooth 1 region in the rift axis (Figure 3a).

The 159ROV dive followed a 1.6 km long south-north track (Figure 3b) on the Smooth 1 volcanic area between 8°48.2′S and 8°47.4′S and crossed the pillow mound (see Figure 2) in the rift axis. The area south of the pillow mound is characterized by lobate lava and sheet flows that are disrupted by distinct flows of pillow lava or jumbled sheet flows (Figure 3b, photos a–c). The sediment cover in this area is relatively thick on the pillow and lobate flows but seems to decrease on the overlying jumbled flow (Figure 3a, photo b) and to the north to the base of the pillow mound. During the dive south of the axial pillow mound, the ROV traversed four boundaries between lava flows with different morphologies (Figures 4e and 4f) that probably represented different eruption events. All lavas sampled from this region south of the axial pillow mound are aphyric to slightly olivine-phyric (Table 1). Although the Smooth 1 area is highly reflective in the sidescan sonar map, ROV observations show abundant sediment patches on the lavas (Figure 3b). The pillow

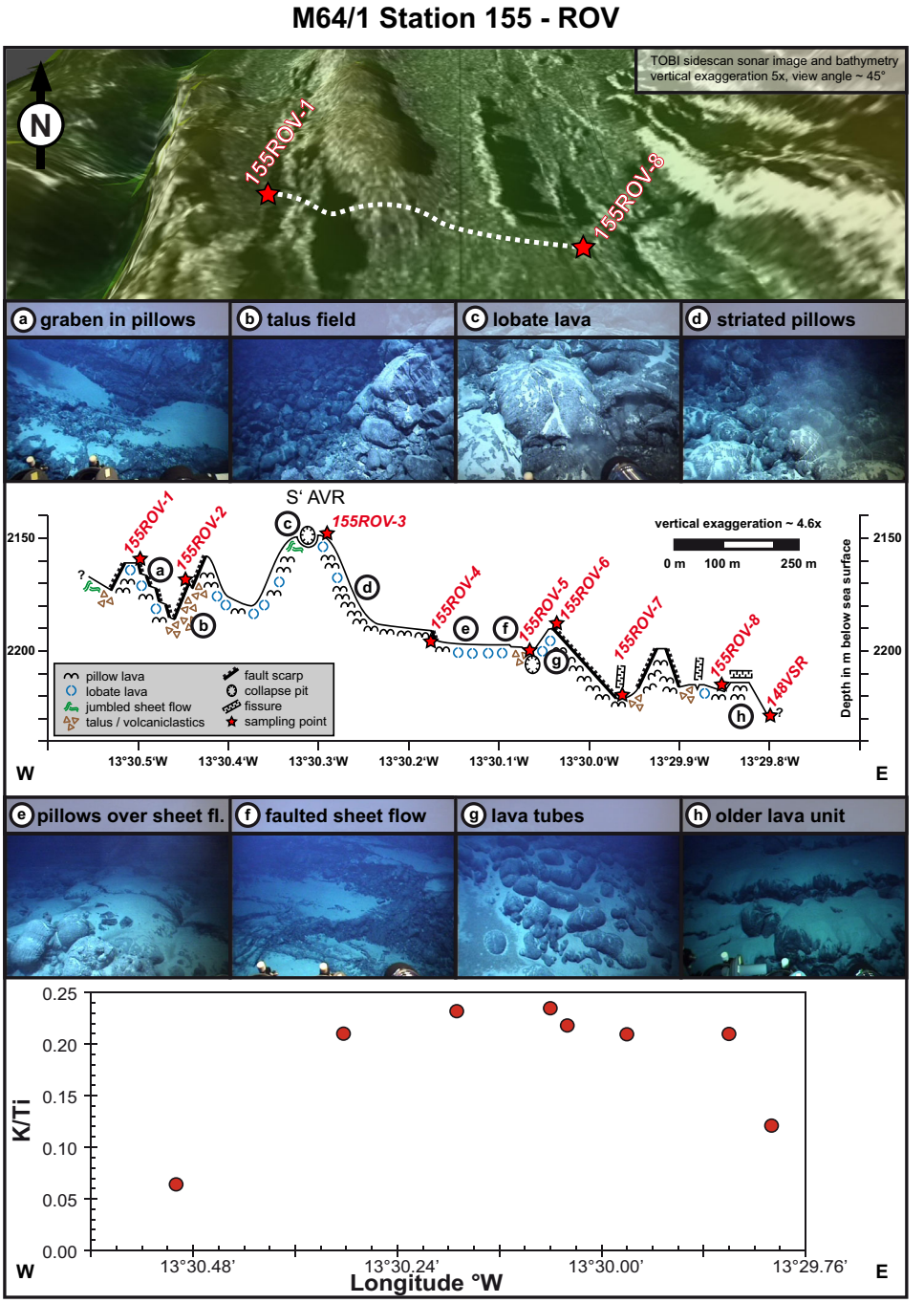

Figure 3. Geology of the rift valley at the Mid-Atlantic Ridge near 8°48′S as observed during the dives (a) 155ROV perpendicular and (b) 159ROV parallel to the rift. We show the observations of volcanic and tectonic structures as well as the sampling locations along the tracks. Representative photographs are shown for the two dive tracks. Note also the variation of the K/Ti ratios in the sampled glasses across the rift zone of 155ROV with the older rift flank lavas having lower K/Ti than the young lavas from the rift axis.

mound is 400 m in diameter and consists entirely of pillow lavas and some single elongated pillows with an eruptive fissure or pit at the top (Figure 3b, photo d). The basalts of this pillow mound contain abundant plagioclase (~10%) up to 10 mm (Table 1). Depressions in the lava surface are filled by sediment and typically, Gorgonariae (horn coral) grow on the steep flanks of the volcanic mound. North of the pillow mound, lava flow morphologies are dominated by lobate and pillow lava that were observed to cover sheet and jumbled sheet flows in some areas (Figures 3b and 4). The basalts are poorly olivine and plagioclase-phyric (Table 1). Camera observations indicate three different lava flows along this part of the ROV profile where

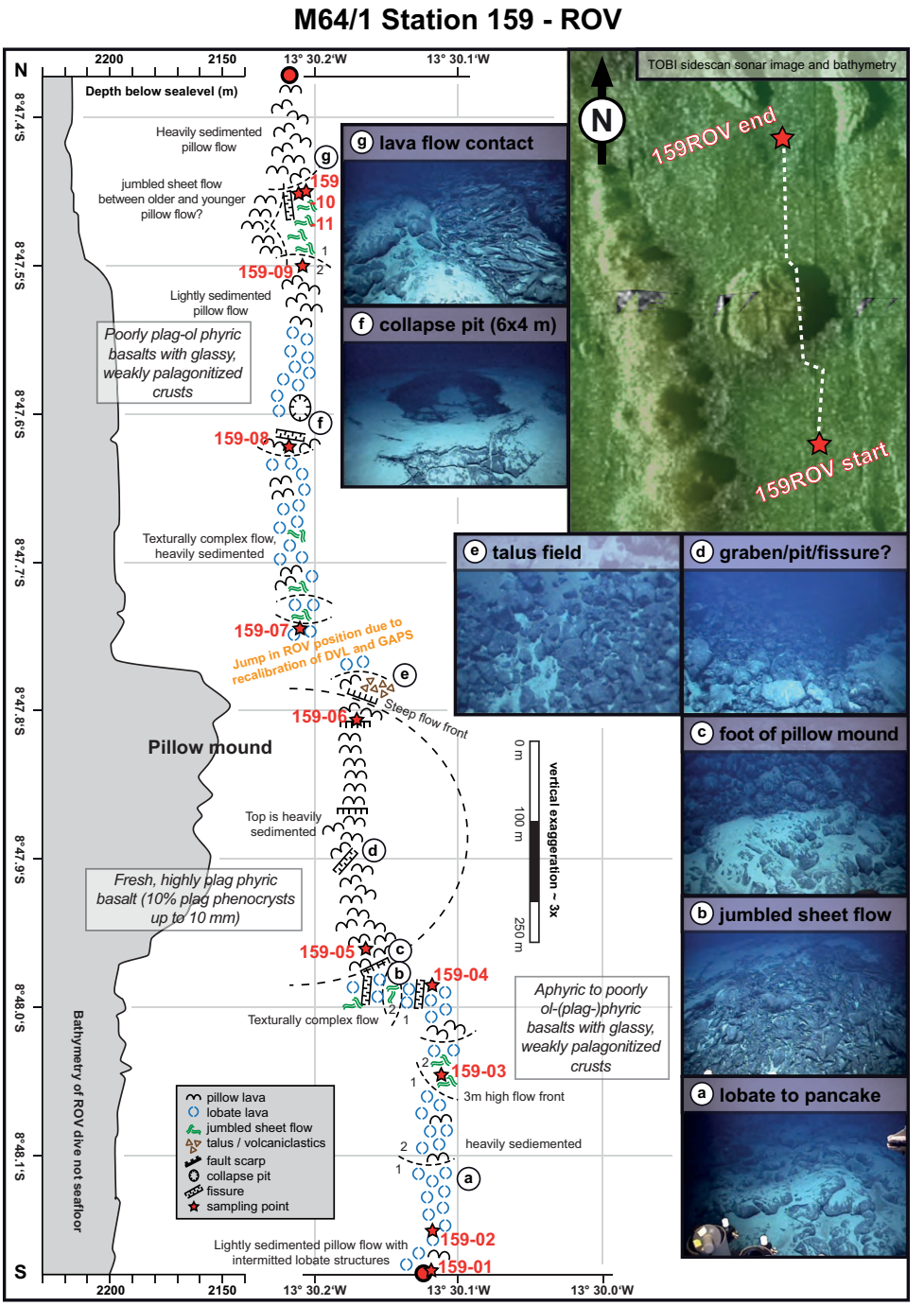

Figure 3. Continued

the lava flow contacts can be determined due to changes in lava morphology and sediment cover (Figure 3b). This dive recovered four samples from lava flows south of the axial pillow mound, two from the pillow mound and another five samples from the lava flows north of the mound (Figure 3b).

4.2. Petrography of the Lavas

All lavas are fresh and have glassy rims with thin palagonite and Mn-Fe oxide staining and descriptions are provided in Table 1. Most lavas from the Smooth 1 volcanic area are aphyric or slightly olivine-phyric with little plagioclase but some lavas with larger amounts of plagioclase and rarely clinopyroxene were

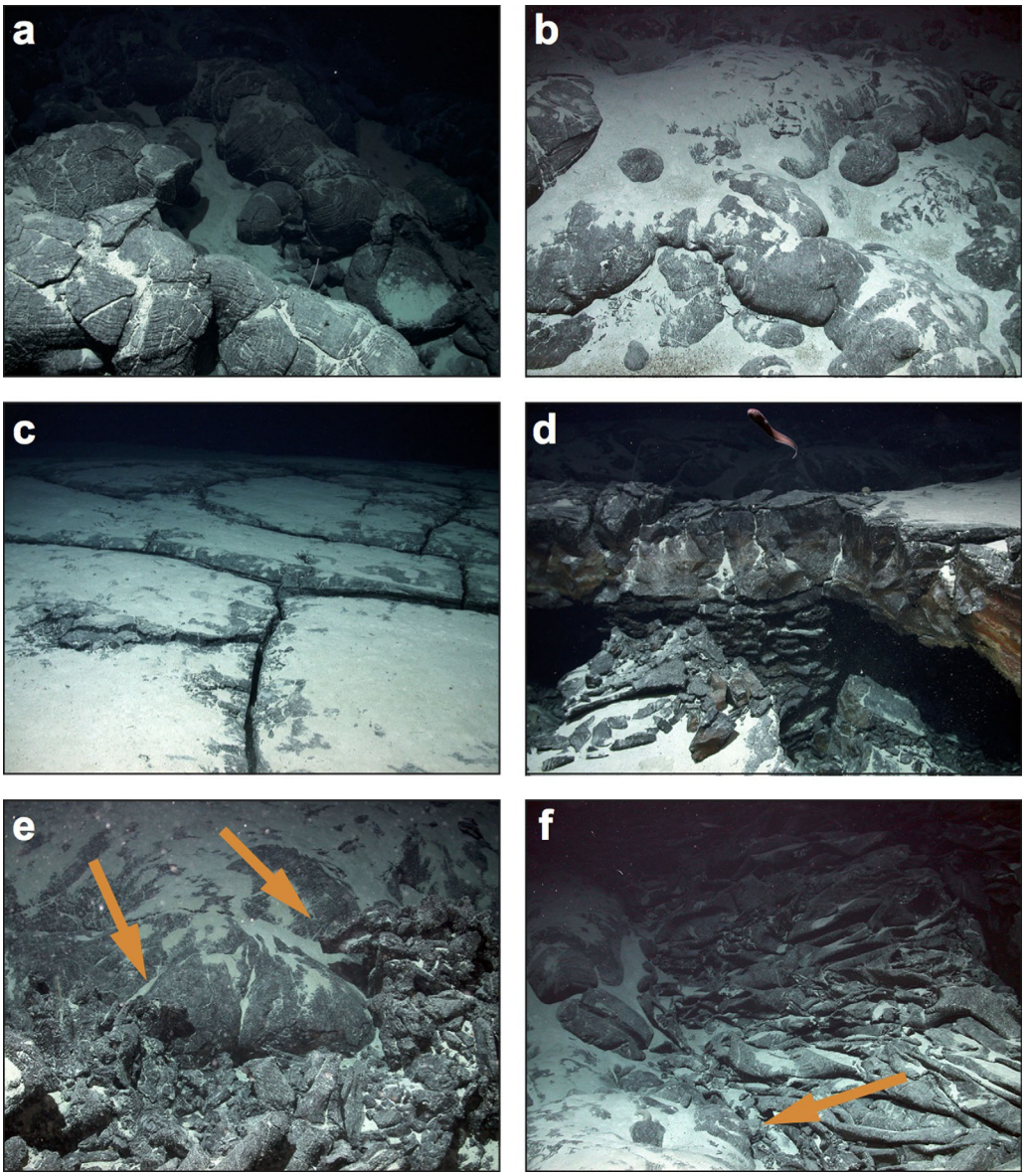

Figure 4. Photographs of representative lavas from the ROV dives (for location of dives see Figure 1). (a) Typical pillow lavas with sediment pockets. (b) Pillow lavas and lava tubes. (c) Sediments on sheet flow. (d) Lava pillar in collapse pit. (e) Contact between pillow lava overlying a sedimented lobate lava flow (orange arrows mark the contact). (f) Jumbled sheet flow overlying sedimented pillow lavas (orange arrow points to contact).

recovered. The samples from the older large axial pillow volcano at 8°48′S and those from the western rift flank contain significant amounts of plagioclase phenocrysts with sizes up to 10 mm (Table 1). Olivine and plagioclase are the most abundant phenocryst phases but clinopyroxene was observed in a few samples (e.g., 159ROV-5 and 159ROV-11). Olivine crystals are generally euhedral to skeletal and homogeneous in composition and range from Fo83 to 88. Plagioclase is also euhedral to skeletal and much more variable in composition both across the area (in the range An69.6 to 89.5) and within individual samples, e.g., plagioclase in 159ROV-11 shows zoning from cores with An89.5 to rims with An74.3. Phenocryst sizes range up to 10 mm for plagioclase whereas the other minerals are generally smaller. Cr-spinel with Mg# of 50–56 and Cr# of 45–52 occurs as inclusions in olivine and clinopyroxene.

4.3. Compositions of the Volcanic Glasses

The lavas sampled in the Smooth 1 area of the rift axis show a compositional variation with MgO contents ranging from 8.5 to 4.5 wt % (Figure 5). The glasses recovered from the Hummocky 1 area, i.e., those from

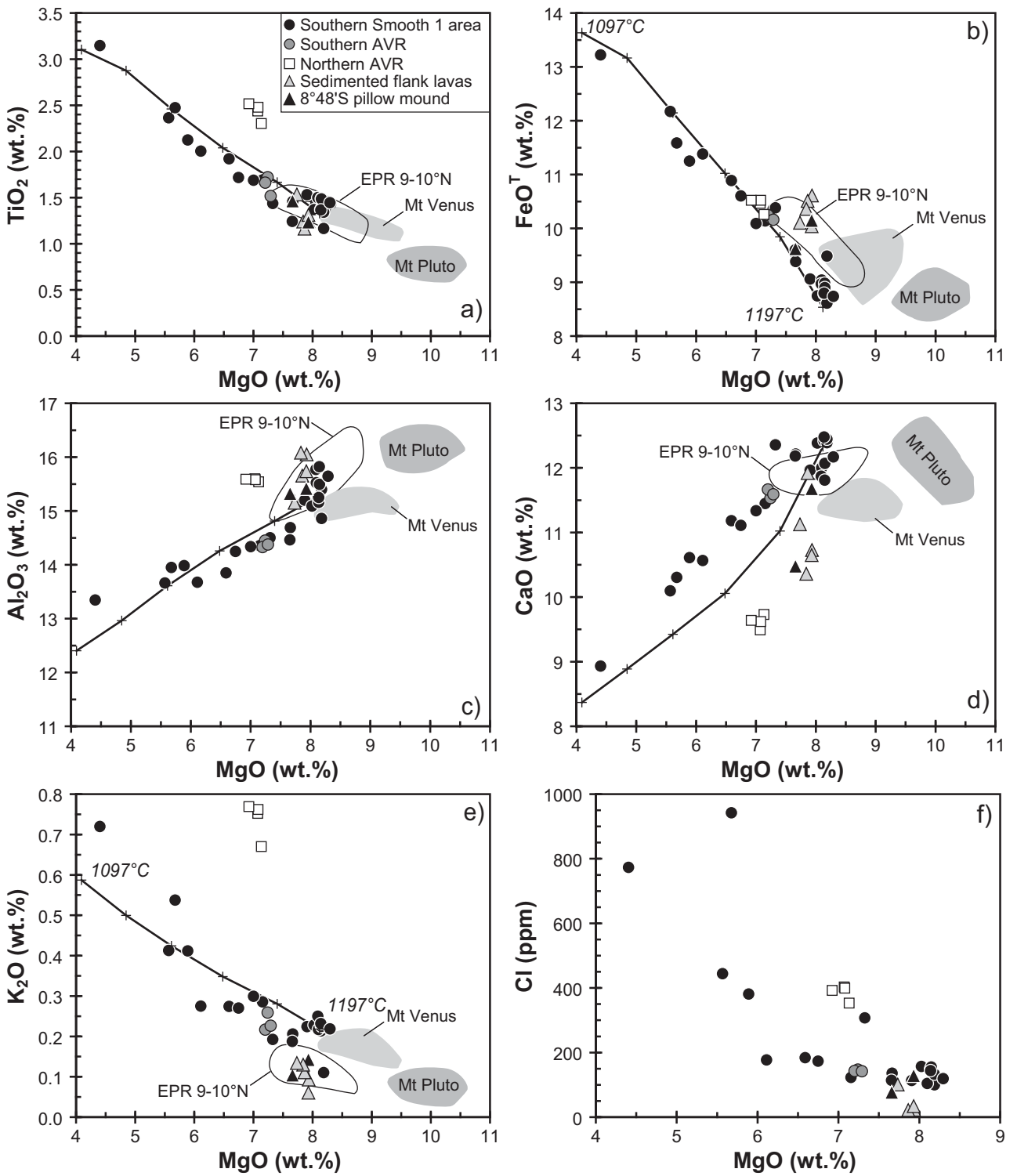

Figure 5. Major element diagrams of glass samples of lavas from the area of the lava flow at 8°48′S on the Mid-Atlantic Ridge. Note that the samples from the rift flanks and the axial pillow mound are more depleted in K_2O than the young lavas from the axial lava flows. The lavas from the northern axial volcanic ridge (AVR) are more enriched in K_2O than the southern AVR and smooth area lavas. The glasses from the southern AVR and Smooth 1 area lavas lie along one liquid line of descent and are probably genetically related. The line shows a MELTS model curve for crystal fractionation at 0.1 GPa with a primitive basalt having the composition of sample 155ROV-5 with 0.2 wt % water. The model supports significant fractionation processes and a temperature range of the erupted liquids between 1197°C and 1097°C with tick marks indicating steps of 20°C. Also shown are fields for glass compositions from the AVRs Mt. Pluto and Mt. Venus on the MAR at 36°49′N [*Bryan and Moore*, 1977; *Stakes et al.*, 1984] and the youngest eruptions on the East Pacific Rise between 9°N and 10°N [*Waters et al.*, 2013].

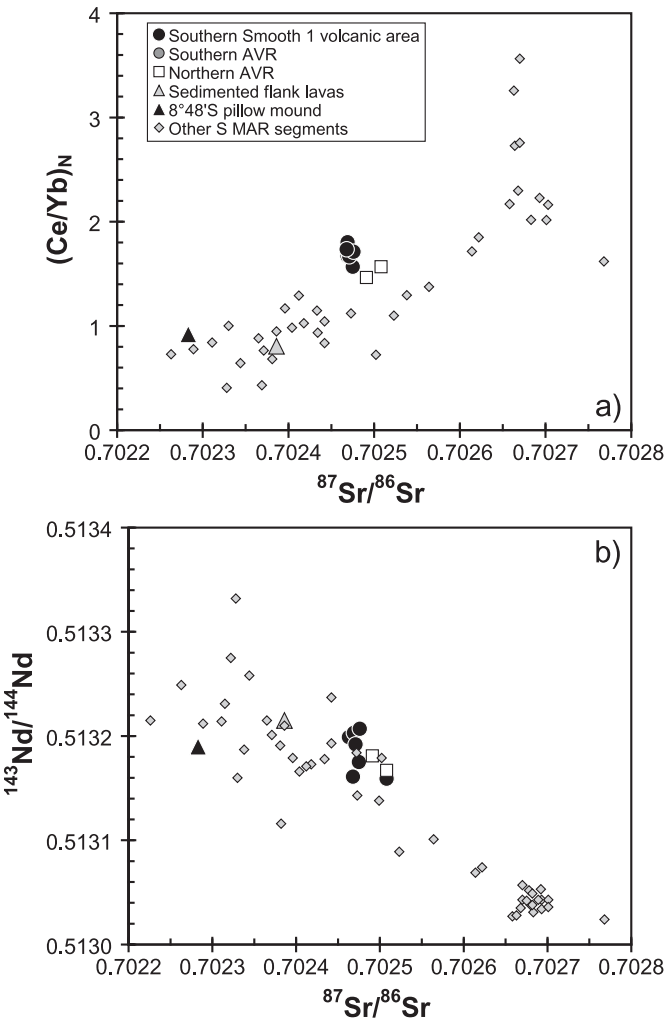

Figure 6. Variation of (a) $(Ce/Yb)_N$ versus $^{87}Sr/^{86}Sr$ and (b) $^{143}Nd/^{144}Nd$ versus $^{87}Sr/^{86}Sr$ of the five different lava units in comparison to the range observed along all four segments of the MAR between 7°S and 12°S [*Hoernle et al.*, 2011]. Note that the lavas from the young axial rift lavas have similar isotopic compositions but differ in incompatible element ratios like $(Ce/Yb)_N$ and most notably in K/Ti (Figure 8).

the AVRs show significant variations and we find, for example, that glasses from the northern AVR have higher TiO_2 and K_2O at similar MgO contents than those from the southern AVR (Figures 5a and 5e). Consequently, five different groups of magmatic glasses can be distinguished in terms of TiO_2, K_2O, CaO, and geographical occurrence. These are (1) samples from the southern AVR, (2) lavas from the Smooth 1 area surrounding the southern AVR, (3) lavas from the northern AVR, (4) lavas from the sediment-covered rift flank, and (5) samples from the large pillow mound within the axis (Table 1). Many of the glass samples from the southern AVR and the surrounding Smooth 1 volcanic area have 6–8.5 wt % MgO and intermediate K_2O of 0.2–0.3 wt %, although a few more evolved samples show an increase of K_2O to contents of 0.7 wt % with decreasing MgO (Figure 5e). One exception is sample 159ROV-2 that was recovered in the southern Smooth 1 volcanic area but has a low K_2O content of 0.11 wt %. The three samples recovered on the southern AVR have similar MgO and K_2O contents of about 7.2 wt % and 0.22–0.26 wt %, respectively (Figure 5). The samples from the southern AVR and the surrounding Smooth 1 area lie along linear trends of increasing FeO^T, TiO_2, and K_2O and decreasing CaO and Al_2O_3 between 4.4 and 8.5 wt % MgO (Figures 5a–5d). In contrast, lavas sampled along the northern AVR (160VSR to 163VSR) all have compositions with about 7 wt % MgO but have higher TiO_2, Al_2O_3, and K_2O and lower CaO than the southern lavas (Figure 5). Two samples recovered from the large pillow mound at 8°48′S and five glasses from the heavily sediment-covered flanks of the axial rift volcanic area have lower K_2O contents than the glasses of the southern AVR and Smooth 1 area (Figure 5d). The glasses from the sediment-covered rift flank also have lower CaO and higher Al_2O_3 than the samples from the southern axial rift (Figures 5d and 5c). The Cl concentrations in most southern lavas remain constant between 6 and 8.4 wt % MgO but increase at lower MgO. Most glasses from the pillow mound and from the sediment-covered lavas at the rift flanks have lower Cl contents than the southern axial rift samples but lavas from the northern AVR basalts have higher Cl for a given MgO (Figure 5f). All lavas show increasing S contents with decreasing MgO. All lavas from the young volcanic area in the axial rift except those from the pillow mound have similar $(Ce/Yb)_N$, $^{87}Sr/^{86}Sr$, and $^{143}Nd/^{144}Nd$ (Figure 6). The lavas from the pillow mound and from the heavily sedimented rift flank are slightly depleted in the light rare earth elements with $(Ce/Yb)_N < 1$ and have lower $^{87}Sr/^{86}Sr$ at similar $^{143}Nd/^{144}Nd$. They resemble the relatively depleted lavas from the portion of the MAR between 7°S and 12°S.

All glasses from the Mid-Atlantic Ridge near 8°48′S have $(^{230}Th/^{238}U) > 1$ and the incompatible element-depleted samples from the heavily sedimented rift flanks and the large axial pillow mound display the

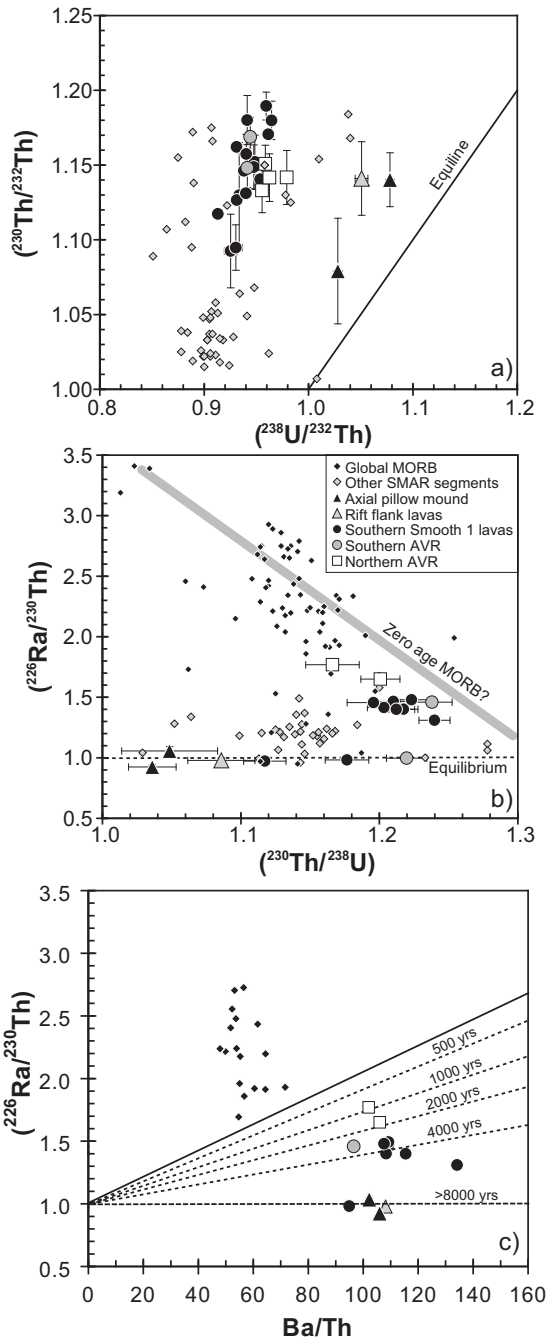

Figure 7. Variation of the (a) (^{230}Th/^{232}Th) versus (^{238}U/^{232}Th), (b) (^{226}Ra/^{230}Th) versus (^{230}Th/^{238}U), and (c) (^{226}Ra/^{230}Th) versus Ba/Th for the A2 lavas following the model of *Rubin and Macdougall* [1990]. Zero-age MORB from recent eruptions on the East Pacific Rise (EPR), the MAR, and the Gorda Ridge [*Cooper et al.*, 2003; *Lundstrom et al.*, 1999; *Rubin et al.*, 2005; *Sims et al.*, 2002; *Waters et al.*, 2013] are shown to estimate the possible initial (^{226}Ra/^{230}Th) at a given (^{230}Th/^{238}U) for the Mid-Atlantic Ridge lavas. The line in Figure 7b is a regression through the zero-age U series isotope data from the EPR that are assumed to represent the initial disequilibria. The lines in Figure 7c indicate different ages assuming an initial (^{226}Ra/^{230}Th) of two. A higher initial (^{226}Ra/^{230}Th) of three would increase the ages by about 1000 years whereas a lower initial (^{226}Ra/^{230}Th) would lead to lower calculated ages. The error bars in (^{226}Ra/^{230}Th) are smaller than the symbols due to the large scale.

lowest disequilibria <1.1 (Figure 7). Compared to the lavas recovered along the MAR between 7° and 12°S, the samples from the study area at 8°48′S have the highest Ra excesses (Figure 7). (^{226}Ra/^{230}Th) is variable in the different lava units where the lavas from the northern AVR have the highest disequilibrium of about 1.7, and most glasses from the southern Smooth 1 volcanic area and one from the southern AVR unit have (^{226}Ra/^{230}Th) of about 1.4 (Figure 7b). The samples from the old lavas but also two from the southern volcanic smooth area and one from the southern AVR are in equilibrium in terms of (^{226}Ra/^{230}Th).

4.4. Along Axis Variations of Compositions

The MgO contents of the southern Smooth 1 lava unit show systematic variations with latitude, with the highest MgO in the center of this area and lower MgO at the northern and southern ends (Figure 8a). In contrast, the northern AVR lavas, the samples from the pillow mound, and the glasses from the rift flank have relatively constant and elevated MgO. Compositional differences between the different lava units are also observed in K/Ti and $(Ce/Yb)_N$, with glasses from the northern AVR having the highest K/Ti but intermediate $(Ce/Yb)_N$ whereas the lavas from the rift flank are much more depleted than the axial lava units (Figures 8b and 8c). Most glasses have similar $Cl/K < 0.07$ but the more evolved glasses at the northern and southern ends of the southern Smooth 1 lava flows show more variation and higher Cl/K ratios (Figure 8d).

5. Discussion

5.1. Definition and Formation of the Lava Units

Although the lavas in the 8°48′S area all show the same strong acoustic reflectivity in the TOBI map (Figure 1c) and thus apparently represent the youngest lavas observed along the axial rift of the A2 segment, the geochemical data indicate significant differences between the lavas from different areas of this volcanic region (Figure 5). The two rows of volcanic cones (Figures 1c and 2) are similar to the AVRs described previously from the Mid-Atlantic Ridge [*Head et al.*, 1996; *Smith and Cann*, 1993] and in terms of their lengths and heights they closely resemble Mt. Pluto and Mt. Venus in the FAMOUS area [*Ballard and Andel*, 1977]. Their elongated shape suggests that these ridges probably formed

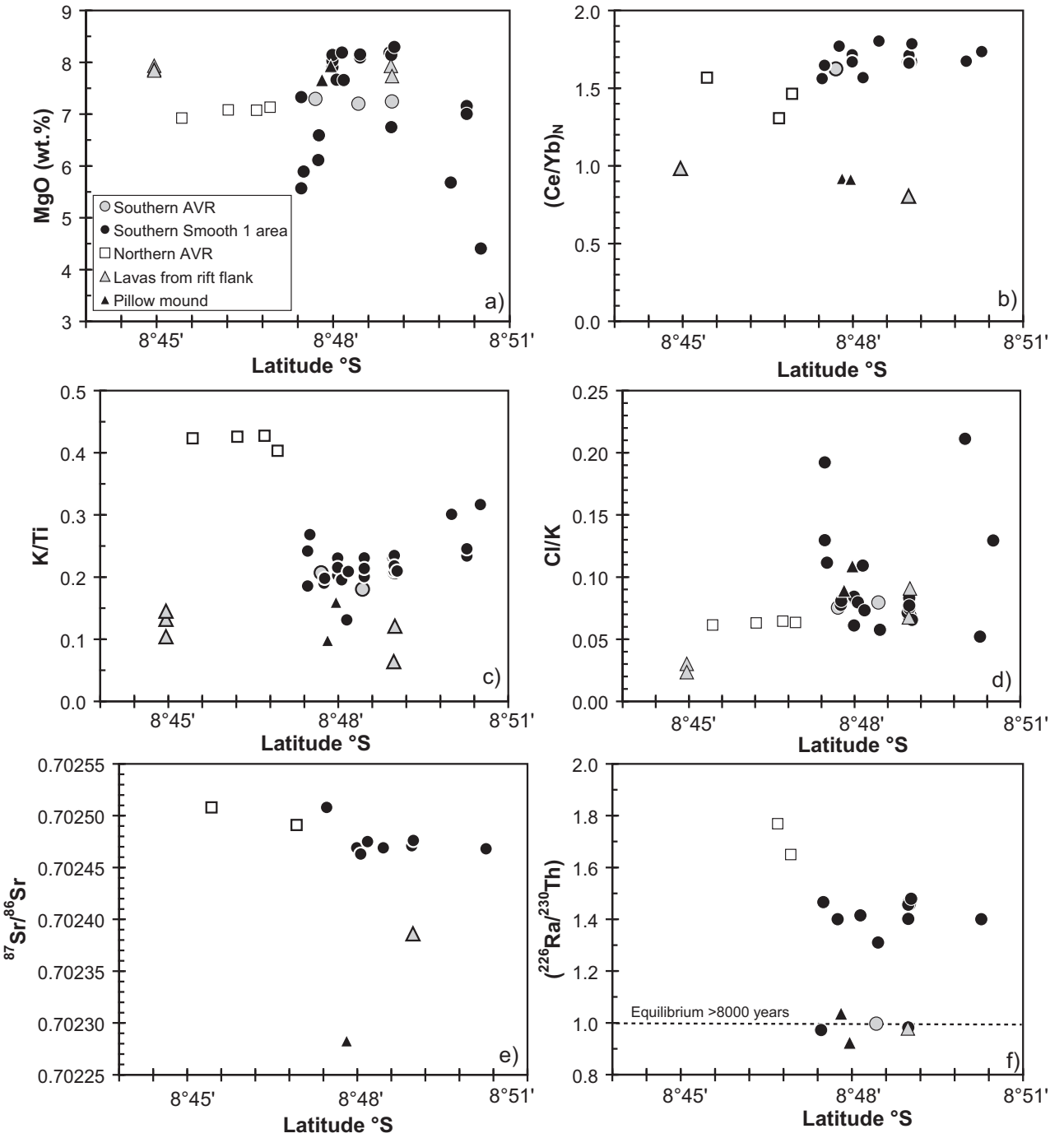

Figure 8. The compositions of (a) MgO, (b) $(Ce/Yb)_N$, (c) K/Ti, (d) Cl/K, (e) $^{87}Sr/^{86}Sr$, and (f) $(^{226}Ra/^{230}Th)$ of the basaltic glasses versus latitude showing the along-axis variations of the different lava units on the Mid-Atlantic Ridge near 8°48′S. Note that the glasses from the axial volcanic ridges (AVR) have very homogeneous compositions indicating that the final eruptions of each AVR yielded similar melts along the entire fissure.

above dikes and represent the products of fissure eruptions [*Head et al.*, 1996; *Thordarson and Larsen*, 2007]. The similar composition of the four samples from the northern AVR (Figure 5) and of the three glass samples from the southern AVR indicates that in both cases the entire ridge produced similar lavas during their emplacement. The compositional similarity of the glasses from the southern AVR to some of the lavas from the southern Smooth 1 lava unit (Figure 5) suggests that the lava of this unit erupted from the AVR. These observations are comparable to those from Iceland, where rows of volcanic cones from fissure eruptions are

the source of extensive lava flows [e.g., *Eason and Sinton*, 2009]. Alternatively, the lava flows may have erupted later and covered the region around the AVRs (kipukas). However, because one southern AVR sample has a (^{226}Ra/^{230}Th) of about 1.5 similar to the southern Smooth 1 lavas (Figure 7b), we suggest that both the AVR and the surrounding lavas formed within a relatively short period of time. Based on the variations in major elements like CaO, Al_2O_3, TiO_2, and K_2O, the young axial lavas from the Humocky 1/Smooth 1 region can be grouped into the northern AVR samples and those from the southern AVR and its surrounding lava flows. The older basalt glasses from the rift flank are more depleted in incompatible elements and have lower K_2O contents as well as low K/Ti and $(Ce/Yb)_N$. The solitary large axial pillow mound occurring within the Smooth 1 lava flows shows the same geochemical composition as the older lavas on the rift flanks (Figure 5). Two samples from this pillow mound also have (^{226}Ra/^{230}Th) of 1 whereas the surrounding lavas of the Smooth 1 area have Ra excess (Figure 7). Consequently, we suggest that this pillow mound belongs to the older lavas and was surrounded by younger flows.

The observed variations indicate different parental magmas for the northern and southern lavas, and variable degrees of crystal fractionation within the southern AVR and Smooth 1 melts (Figure 5). This implies that the eruptions formed from several relatively small batches of magma rising independently through the crust within a relatively short period of time. It also indicates that the mantle beneath this segment is heterogeneous on a small scale of a few kilometers. Incompatible element ratios and radiogenic isotopes indicate a northward-directed trend of decreasing enrichment in the lavas along the A2 segment [*Hoernle et al*., 2011]. However, the lavas of the young field do not fit into this regional trend. Rather, the northern lavas are more enriched in K than the southern lavas (Figure 5e) contrary to what is observed on the broader scale [*Hoernle et al*., 2011]. Variations of lava compositions were also found at other regions of the MAR like, for example, in the FAMOUS and MARNOK segments [*Bryan and Moore*, 1977; *Lawson et al*., 1996; *Stakes et al*., 1984] and closely related lava successions on the East Pacific Rise show significant variation in radiogenic isotope and incompatible element ratios indicating mixing between depleted and enriched sources [*Bergmanis et al*., 2007; *Waters et al*., 2013]. Thus, melting along both fast and slow spreading ridges samples chemically and isotopically variable portions of the mantle.

By surface area, the southern Smooth 1 lava unit is the most extensive and occurs over a distance of 7 km between 8.79°S and 8.84°S, possibly overlapping with lava flows surrounding the northern AVR. Although the Smooth 1 area is highly reflective in the side scan map (Figure 1c), the ROV observations reveal variations in the thickness of the sediment cover on the lavas, but the lavas are always visible in the central part of the rift. The widest area of lavas occurs east of the southern AVR with a width of about 2 km and the whole southern Smooth 1 and southern AVR lava unit covers an estimated 9 km^2 but the boundaries to the northern lavas is unknown. The composition of the smooth lava flows surrounding the about 3 km long northern AVR is not clear. Here the lava flows occur within a width of perhaps 1.5 km, thus covering about 5 km^2. The area covered by one eruption could range from about 5 km^2 for one subunit to 14 km^2 for the entire Smooth 1 area which is comparable to lava flows on the Galapagos Rise ($<$1 to 14.6 km^2 [*Colman et al*., 2012]), the East Pacific Rise (0.8–18 km^2 [*Sinton et al*., 2002; *Soule et al*., 2007]), or Axial Seamount (2–7.8 km^2 [*Clague et al*., 2013]), but less than the lava flows surrounding Icelandic volcanoes that cover some 24 to more than 100 km^2 [*Eason and Sinton*, 2009; *Rossi*, 1997; *Thordarson and Self*, 1993]. Thus, the areas of lava flows erupting at the slow spreading MAR appear to be similar to those at intermediate to fast spreading axes like the East Pacific Rise or the Galapagos Rise.

5.2. Composition and Petrogenesis of the Southern Axial Rift Lavas

The variation of MgO contents in the glasses recovered from the southern AVR and southern Smooth 1 lava unit range between 8.5 and 4.5 wt % (Figure 5). This is larger than variations in glasses from other detailed studies on the MAR, the East Pacific Rise, and the Galapagos Spreading Center, which typically have MgO higher than 6 wt % [*Colman et al*., 2012; *Sinton et al*., 2002; *Waters et al*., 2013] For example, sampling of the two AVRs of Mt. Pluto and Mt. Venus on the MAR at 36°49′N [*Bryan and Moore*, 1977] revealed very primitive and homogeneous lava compositions (Figure 5). Similarly, very young lava units on the EPR at 9°N–10°N [*Waters et al*., 2013] have a relatively restricted composition in terms of MgO (Figure 5).

Because all glasses from the southern Smooth 1 and AVR lava units lie on relatively tight linear trends in TiO_2, Al_2O_3, CaO, and K_2O (Figure 5), have similar $(Ce/Yb)_N$ as well as Sr isotope ratios, and mostly identical (^{226}Ra/^{230}Th) implying similar ages, we used MELTS [*Ghiorso*, 1997] modeling to investigate the hypothesis

that they lie on a single liquid line of descent (LLD). Evidence for magma lenses is rare beneath the MAR but a seismic study revealed the presence of melt beneath an AVR at 57°45′N at a depth of 2.5 km below the sea surface [*Sinha et al*., 1998]. We assume that a magma body was present at similar depths beneath the AVR at 8°48′S where the melts may have undergone fractional crystallization. Primitive MORB probably have oxygen fugacities around the quartz-fayalite-magnetite (QFM) buffer [*Cottrell and Kelley*, 2011] and contain low contents of water [*Almeev et al*., 2008]. A calculated LLD for crystal fractionation at 0.1 GPa, 0.2 wt % H_2O, and an oxygen fugacity at QFM is shown on Figure 5. We conclude that the glasses from the southern Smooth 1 lava flows erupted from the southern AVR and represent liquids that underwent different amounts of fractional crystallization at depths of about 3 km but formed from similar parental magmas. Because most of these lavas have similar Ra excesses (Figure 7), they probably resulted from the same melting and eruption event.

Because MgO, CaO, and Al_2O_3 all decrease, the fractionated phases must be olivine, clinopyroxene, and plagioclase that are the most abundant mineral phases in the samples, and the fractionation assemblage suggested by the MELTS model. The decreasing MgO contents at the northern and southern end of the southern Smooth 1 and AVR lava unit indicate that melts at the edges of the magma system apparently stagnated and cooled for longer periods of time in the crust than in the center of the magma system. The MELTS model (Figure 5) suggests that the most evolved melt composition is some 100°C cooler than the most mafic magma implying significant temperature variations in the magma system. Interestingly, we also observe higher Cl/K in the lavas at the two ends of the eruptive unit, implying more extensive assimilation of hydrothermally altered crustal material coupled to extensive fractionation in a crustal reservoir. Although these crustal magma reservoirs are probably only temporary active at slow spreading ridges they may contain variably evolved and crustally contaminated liquids similar to the melt lenses beneath fast spreading ridges [*Coogan et al*., 2003; *Freund et al*., 2013; *Gillis et al*., 2003]. A systematic MgO decrease from 8.5 wt % at the segment center to 6.5 wt % at the segment ends was observed in volcanic glasses sampled along the segment at about 24°N of the Mid-Atlantic Ridge and is believed to reflect lateral dike intrusion [*Lawson et al*., 1996]. We suggest that magma erupting at the center of the southern Smooth 1 and southern AVR lava unit was relatively hot and ascended from the center of the magma intrusion. In contrast, magmas that erupted at the ends of the Smooth 1 lava flows possibly rose from the tips of the crustal reservoir, where they cooled, fractionated, and assimilated more than the melts in the intrusion center.

5.3. Constraints on Eruption Ages Using (^{226}Ra/^{230}Th) and (^{230}Th/^{238}U)

Short-lived isotopes like ^{230}Th and ^{226}Ra can be used to approximate ages of lavas [*Rubin and Macdougall*, 1990; *Sturm et al*., 2000]. Global MORB lie on a negative trend in terms of (^{226}Ra/^{230}Th) and (^{230}Th/^{238}U), and most of the glasses from the MAR at 8°48′S lie at the end with relatively high ^{230}Th but low ^{226}Ra excesses (Figure 7b). Compared to most lavas recovered from the MAR between 7°S and 12°S, the glasses sampled near 8°48′S have the highest (^{226}Ra/^{230}Th) and (^{230}Th/^{238}U) (Figure 7) that probably indicate the youngest volcanic activity in the entire region. The variation of the U series isotopes and the Sr-Nd-Pb isotopes along the MAR between 7°S and 12°S most likely reflects mixing of melts from spinel peridotite and from a recycled mafic component [*Hoernle et al*., 2011; *Turner et al*., 2015]. However, the volcanic glasses with Ra excesses from the area at 8°48′S show little variation in terms of Sr and Nd isotope ratios and Ba/Th (Figures 6 and 7) implying a relatively homogeneous mantle source and thus no significant effects of variable mantle components on the initial (^{226}Ra/^{230}Th). The (^{226}Ra/^{230}Th) values of the samples from 8°48′S indicate at least three different volcanic eruption events and in general, the different ages correspond to the groups defined by geographical and compositional means (Figures 5 and 8). Most of the lavas from the AVRs and the southern Smooth 1 lava unit show significant Ra excess indicating an age of much less than 8000 years whereby the northern AVR unit has the highest excess (Figure 7). However, there are three samples from the southern AVR and Smooth 1 lavas that are in equilibrium and, thus, must be older than 8000 years. This implies that lavas with similar composition erupted over an extended period of time. All of the depleted lavas from the rift flanks and the axial pillow mound have also (^{226}Ra/^{230}Th) of 1 and, thus, must also be older than 8000 years. *Rubin and Macdougall* [1990] suggested that the variation of (^{226}Ra/^{230}Th) relative to Ba/Th can be used to estimate the ages of MORB. We find that most of the lavas from the young lava flows at 8°48′S on the MAR have high Ba/Th of 100 $\pm$ 10 (Figure 7c) implying that they also should all have had similar initial (^{226}Ra/^{230}Th), because Ra behaves similarly to Ba during partial melting. According to this model, the lavas from the northern AVR would be the youngest because they have the highest (^{226}Ra/^{230}Th). Zero-age

MORB from the East Pacific Rise, the MAR, and the Gorda Ridge lie on a negative trend of (^{226}Ra/^{230}Th) and (^{230}Th/^{238}U) (Figure 7b) suggesting that basalts with high (^{230}Th/^{238}U) have relatively low (^{226}Ra/^{230}Th). Based on the estimated compositions of zero-age MORB in Figure 7b, our samples could have initial (^{226}Ra/^{230}Th) between 1.7 and 2.2. Taking a median value of (^{226}Ra/^{230}Th) = 2 implies an age of about 1000–2000 years for the northern AVR lavas and ages of about 4000 years for the southern AVR and Smooth 1 lava units (Figure 7c). In view of the assumptions, we have made to determine the initial (^{226}Ra/^{230}Th), these ages may have an error of about ±1000 years (an initial (^{226}Ra/^{230}Th) ratio of 3, for example, would lead to ages that are about 1000 years older). The analytical errors for (^{226}Ra/^{230}Th) are less than 0.04 (2 SE), i.e., smaller than the symbols in Figure 7 and thus negligible. These ages are all considerably younger than the roughly 10,000 years suggested for the Serocki volcano and AVR on the northern Mid-Atlantic Ridge where all lavas showed (^{226}Ra/^{230}Th) equilibrium [*Sturm et al*., 2000]. We suggest that eruptive events on the MAR at 8°48′S occurred after volcanic repose times of 2000 to more than 4000 years. Time periods of several 1000 years between volcanic eruptions are somewhat shorter than those suggested for slow spreading segments with normal thickness of 7.0–7.5 km where tectono-magmatic cycles with periods of 10,000–100,000 years and transient magma bodies were suggested [*Sinha et al*., 1998]. The observation of small faults within the southern Smooth 1 lava flows indicates tectonic movement after the extrusion (Figure 3) implying that volcanism is not very recent, in agreement with ^{226}Ra excesses, the observed sediment patches, and the absence of signs of hydrothermal activity either on the seafloor (with the ROV) or from turbidity in the water column. The presence of faulting appears to confirm longer repose times of several 1000 years between volcanic eruptions that appear to be significantly longer at the slow spreading MAR than those of only tens of years observed at the fast spreading EPR [*Bergmanis et al*., 2007; *Goss et al*., 2010] and than decades to centuries at both Axial Volcano [*Clague et al*., 2013] and the Galapagos Spreading Centre [*Bowles et al*., 2014].

More frequent volcanic eruptions at the MAR at 8°48′S than at Serocki volcano are probably related to the melting anomaly and thickened crust at 10°S [*Bruguier et al*., 2003; *Hoernle et al*., 2011]. The enriched mantle material in this region produces more magma and about 10 km thick crust as well as more abundant volcanic eruptions at the surface. Nevertheless, the eruption frequency is significantly lower than that assumed for fast spreading ridges like the East Pacific Rise [*Rubin and Sinton*, 2007]. The different lava ages indicate that the volcanic activity in segment A2 occurs over relatively brief periods of time separated by several thousand years of tectonic activity only. At present, this part of the A2 segment appears to be in a tectonic phase, which is indicated by both faults and abundance of sediments. The chemical differences between the lavas of different age like, for example, between the Smooth 1 rift axis lavas and those from the rift flank imply that magma source compositions on slow spreading axes vary considerably on time scales of several thousand years.

5.4. Magma Ascent Beneath the Axial Rift of the Slow Spreading A2 Segment

Magma ascent to the surface and transport in the shallow crust occurs by diking. A lateral flow of dikes for several tens of kilometers has been observed on Iceland and at Afar [*Björnsson et al*., 1977; *Buck et al*., 2006; *Keir et al*., 2009]. Because slow spreading ridge segments typically show a thickened crust in the segment center models of magma transport suggest long-distance lateral melt transport from the center to the segment ends [*Dunn et al*., 2005; *Grandin et al*., 2012]. A geophysical study on the Reykjanes Ridge indicates that seven AVRs with lengths of 10–30 km were fed by episodic magma intrusion from the mantle [*Peirce et al*., 2005]. The lava flows studied on the MAR at 8°48′S probably erupted from two fissures each about 3 km long that resulted in the formation of the AVRs. The fissures most likely represent surface structures above dikes through the uppermost 2 km of the crust. The geochemical differences between the northern AVR and the southern AVR and surrounding lava unit indicate that the magma reservoirs of the two dikes are separated also at greater depths and that they tap different sources in the mantle. It appears that magma transport from the melting region in the mantle occurs primarily vertically and lateral transport in the crust is restricted. Although seismic work elsewhere on the Mid-Atlantic Ridge has indicated large connected magma systems beneath the axis [*Magde et al*., 2000], the compositional variation on the scale of few kilometers observed at the 8°48′S axial rift indicates that the ascending magmas do not mix during ascent. Consequently, we suggest that melt transport to the surface at the MAR at 8°48′S is largely vertically from the melting region in the mantle rather than laterally from the segment center in the south.

The K/Ti ratios of the glasses show a rough positive correlation with (^{226}Ra/^{230}Th) suggesting an increasing enrichment in the magmas with decreasing age in this part of the Mid-Atlantic Ridge (Figure 9). The

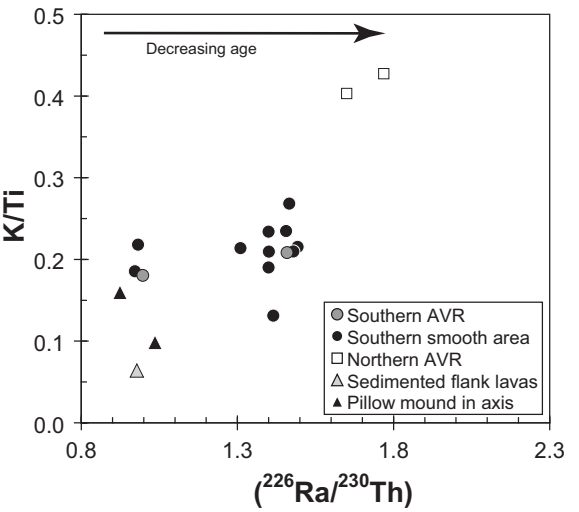

Figure 9. Variation of K/Ti with (^{226}Ra/^{230}Th) for the glass samples from the Mid-Atlantic Ridge at 8°48′S showing that lavas become more enriched with decreasing age.

variation of the lava compositions at 8°48′S on the MAR covers a large portion of the entire range observed along the four segments (Figure 6) indicating mixing between enriched and depleted sources. The variation of K/Ti in the basalts most likely reflects the composition of the mantle beneath the spreading axis because both elements are incompatible in mantle minerals, and K slightly more so than Ti. The observed pattern could thus indicate the northward-directed along-axis flow of enriched mantle from the melting anomaly at 10°S that probably drives the northward-directed ridge propagation of segment A2 [*Bruguier et al.*, 2003]. However, the time period for such along-axis transport appears too short (<100,000 years) because the relatively thicker crust in the A2 segment center of 10 km [*Bruguier et al.*, 2003] implies that excess melting occurred over longer time scales (>500,000 years) at a spreading rate of 33 mm/yr. Thus, the change toward more enriched lava compositions with time may reflect tapping of local sources rather than large-scale northward-directed flow of enriched material from segment A3.

6. Conclusions

A highly reflective and smooth area of about 14 km^2 in the axial rift of the Mid-Atlantic Ridge at 8°48′S represents the youngest volcanic lava succession in the A2 segment with anomalously thick crust. The 8 km long lava formations consist of several lava flows and probably erupted from two fissures underlying the AVRs, each of 3 km length. The southern lavas lie on a liquid line of descent with the lavas from the southern AVR whereas the samples from the northern AVR indicate a different magma source. The Ra disequilibria suggest that the northern lavas are younger than the southern lavas and indicate eruption frequencies with gaps of several 1000 years. Older lavas from the sediment-covered rift flank and a pillow mound in the rift axis are more depleted in incompatible elements and have lower Sr isotope ratios implying that through time variably enriched magmas formed at this portion of the Mid-Atlantic Ridge. The compositional differences of the young axial rift lavas indicate little lateral movement of magma through the crust but rather batches of magma rise vertically from a heterogeneous mantle.

Acknowledgments
We thank Captain M. Kull and his crew for their help during cruise M64/1 with R/V Meteor and the Bremen ROV team for their excellent work. We gratefully acknowledge the help of P. Appel, B. Mader, and N. Stroncik with the electron beam microprobe and U. Westernströer with ICP-MS analyses. This work was supported by the Deutsche Forschungsgemeinschaft under grant De572/22-1, De572/22-2 and Ha 2568/13-1. All data shown in the figures are given in Table 1 and will be available in PetDB. We thank the reviewers K. Rubin, R. Searle, and B. Dreyer for their constructive reviews that significantly improved the quality of this work.

References

Abelson, M., G. Baer, and A. Agnon (2001), Evidence from gabbro of the Troodos ophiolite for lateral magma transport along a slow-spreading mid-ocean ridge, *Nature*, *409*, 72–75.

Almeev, R. R., F. Holtz, J. Koepke, K. M. Haase, and C. Devey (2008), Depths of partial crystallization of H_2O-bearing MORB: Phase equilibria simulations of basalts at the MAR near Ascension Island (7°-11°S), *J. Petrol.*, *49*, 25–45, doi:10.1093/petrology/egm068.

Baker, E. T., and H. T. Milburn (1997), MAPR: A new instrument for hydrothermal plume mapping, *RIDGE Events*, *8*, 23–25.

Ballard, R. D., and T. H. V. Andel (1977), Morphology and tectonics of the inner rift valley at lat 36°50′N on the Mid-Atlantic Ridge, *Geol. Soc. Am. Bull.*, *88*, 507–530.

Bergmanis, E. C., J. M. Sinton, and K. H. Rubin (2007), Recent eruptive history and magma reservoir dynamics on the southern East Pacific Rise at 17°30′S, *Geochem.Geophys. Geosyst.*, *8*, Q12O06, doi:10.1029/2007GC001742.

Björnsson, A., K. Saemundsson, P. Einarsson, E. Tryggvason, and K. Grönvold (1977), Current rifting episode in north Iceland, *Nature*, *266*, 318–323.

Bowles, J. A., A. Colman, J. T. McClinton, J. M. Sinton, S. M. White, and K. H. Rubin (2014), Eruptive timing and 200 year episodicity at 92°W on the hot spot-influenced Galapagos Spreading Center derived from geomagnetic paleointensity, *Geochem.Geophys. Geosyst.*, *15*(6), 2211–2224, doi:10.1002/2014GC005315.

Brozena, J. M., and R. S. White (1990), Ridge jumps and propagations in the South Atlantic Ocean, *Nature*, *348*, 149–152.

Bruguier, N. J., T. A. Minshull, and J. M. Brozena (2003), Morphology and tectonics of the Mid-Atlantic Ridge, 7°-12°S, *J. Geophys. Res.*, *108*(B2), 2093, doi:10.1029/2001JB001172.

Bryan, W. B., and J. G. Moore (1977), Compositional variations of young basalts in the Mid-Atlantic Ridge rift valley near lat 35°49′N, *Geol. Soc. Am. Bull.*, *88*, 556–570.

Buck, W. R., P. Einarsson, and B. Brandsdottir (2006), Tectonic stress and magma chamber size as controls on dike propagation: Constraints from the 1975–1984 Krafla rifting episode, *J. Geophys. Res.*, *111*, B12404, doi:10.1029/2005JB003879.
Canales, J. P., S. C. Singh, R. S. Detrick, S. M. Carbotte, A. Harding, G. M. Kent, J. B. Diebold, J. Babcock, and M. R. Nedimovic (2006), Seismic evidence for variations in axial magma chamber properties along the southern Juan de Fuca Ridge, *Earth Planet. Sci. Lett.*, *246*, 353–366.
Clague, D. A., et al. (2013), Geologic history of the summit of Axial Seamount, Juan de Fuca Ridge, *Geochem.Geophys. Geosyst.*, *14*, 4403–4443. doi:10.1002/ggge.20240.
Colman, A., et al. (2012), Effects of variable magma supply on mid-ocean ridge eruptions: Constraints from mapped lava flow fields along the Galápagos Spreading Center, *Geochem.Geophys. Geosyst.*, *13*, Q08014, doi:10.1029/2012GC004163.
Coogan, L. A., N. C. Mitchell, and M. J. O' Hara (2003), Roof assimilation at fast spreading ridges: An investigation combining geophysical, geochemical, and field evidence, *J. Geophys. Res.*, *108*(B1), doi:10.1029/2001JB001171.
Cooper, K. M., S. J. Goldstein, K. W. W. Sims, and M. T. Murrell (2003), Uranium-series chronology of Gorda Ridge volcanism: New evidence from the 1996 eruption, *Earth Planet. Sci. Lett.*, *206*, 459–475.
Cottrell, E., and K. A. Kelley (2011), The oxidation state of Fe in MORB glasses and the oxygen fugacity of the upper mantle, *Earth Planet. Sci. Lett.*, *305*, 270–282.
Crisp, J. A. (1984), Rates of magma emplacement and volcanic output, *J. Volcanol. Geotherm. Res.*, *20*, 177–211.
Delaney, J. R., D. S. Kelley, M. D. Lilley, D. A. Butterfield, J. A. Baross, W. S. D. Wilcock, R. W. Embley, and M. Summit (1998), The quantum event of oceanic crustal accretion: Impacts of diking at Mid-ocean Ridges, *Science*, *281*, 222–230.
DeMets, C., R. G. Gordon, D. F. Argus, and S. Stein (1994), Effect of recent revisions to the geomagnetic time scale on estimates of current plate motions, *Geophys. Res. Lett.*, *21*, 2191–2194.
Devey, C. W., K. S. Lackschewitz, and E. Baker (2005), Hydrothermal and volcanic activity found on the southern Mid-Atlantic Ridge, *Eos Trans. AGU*, *86*, 209–212.
Dungan, M. A., and J. M. Rhodes (1978), Residual glasses and melt inclusions in basalts from DSDP Legs 45 and 46: Evidence for magma mixing, *Contrib. Mineral. Petrol.*, *67*, 417–431.
Dunn, R. A., V. Lekic, R. S. Detrick, and D. R. Toomey (2005), Three-dimensional seismic structure of the Mid-Atlantic Ridge (35°N): Evidence for focused melt supply and lower crustal dike injection, *J. Geophys. Res.*, *110*, B09101, doi:10.1029/2004JB003473.
Eason, D. E., and J. M. Sinton (2009), Lava shields and fissure eruptions of the Western Volcanic Zone, Iceland: Evidence for magma chambers and crustal interaction, *J. Volcanol. Geotherm. Res.*, *186*, 331–348.
Freund, S., C. Beier, S. Krumm, and K. M. Haase (2013), Oxygen isotope evidence for the formation of andesitic-dacitic magmas from the fast-spreading Pacific-Antarctic Rise by assimilation-fractional crystallization, *Chem. Geol.*, *347*, 271–283.
Garbe-Schönberg, C.-D. (1993), Simultaneous determination of thirty-seven trace elements in twenty-eight international rock standards by ICP-MS, *Geostand. Newsl.*, *17*, 81–97.
Ghiorso, M. S. (1997), Thermodynamic models of igneous processes, *Annu. Rev. Earth Planet. Sci.*, *25*, 221–241.
Gillis, K. M., L. A. Coogan, and M. Chaussidon (2003), Volatile element (B, Cl, F) behaviour in the roof of an axial magma chamber from the East Pacific Rise, *Earth Planet. Sci. Lett.*, *213*, 447–462.
Goss, A. R., M. R. Perfit, W. I. Ridley, K. H. Rubin, G. D. Kamenov, S. A. Soule, A. Fundis, and D. J. Fornari (2010), Geochemistry of lavas from the 2005-2006 eruption at the East Pacific Rise, 9°46′N-9°56′N: Implications for ridge crest plumbing and decadal changes in magma chamber compositions, *Geochem.Geophys. Geosyst.*, *11*, Q05T09, doi:10.1029/2009GC002977.
Govindaraju, K. (1994), 1994 compilation of working values and sample description for 383 geostandards, *Geostand. Newsl.*, *18*, 1–158.
Grandin, R., A. Socquet, C. Doubre, E. Jacques, and G. C. P. King (2012), Elastic thickness control of lateral dyke intrusion at mid-ocean ridges, *Earth Planet. Sci. Lett.*, *319-320*, 83–95.
Hall, L. S., and J. M. Sinton (1996), Geochemical diversity of the large lava field on the flank of the East Pacific Rise at 8°17′S, *Earth Planet. Sci. Lett.*, *142*, 241–251.
Hanan, B. B., R. H. Kingsley, and J.-G. Schilling (1986), Pb isotope evidence in the South Atlantic for migrating ridge-hotspot interactions, *Nature*, *322*, 137–144.
Head, J. W., L. Wilson, and D. K. Smith (1996), Mid-ocean ridge eruptive vent morphology and substructure: Evidence for dike widths, eruption rates, and evolution of eruptions and axial volcanic ridges, *J. Geophys. Res.*, *101*, 28,265–28,280.
Hoernle, K., F. Hauff, T. F. Kokfelt, K. Haase, D. Garbe-Schönberg, and R. Werner (2011), On- and off-axis chemical heterogeneities along the South Atlantic Mid-Ocean-Ridge (5–11°S): Shallow or deep recycling of ocean crust and/or intraplate volcanism?, *Earth Planet. Sci. Lett.*, *306*, 86–97, doi:10.1016/j.epsl.2011.03.032.
Jochum, K. P., H. M. Seufert, and M. F. Thirlwall (1990), Multi-element analyses of 15 international standard rocks by isotope-dilution spark source mass spectrometry, *Geostand. Newsl.*, *14*, 469–473.
Keir, D., et al. (2009), Evidence for focused magmatic accretion at segment centers from lateral dike injections captured beneath the Red Sea rift in Afar, *Geology*, *37*, 59–62.
Kokfelt, T. F., C. Lundstrom, K. Hoernle, F. Hauff, and R. Werner (2005), Plume-ridge interaction studied at the Galápagos spreading center: Evidence from 226Ra-230Th-238U and 231Pa-235U isotopic disequilibria, *Earth Planet. Sci. Lett.*, *234*, 165–187.
Lawson, K., R. C. Searle, J. A. Pearce, P. Browning, and P. Kempton (1996), Detailed volcanic geology of the MARNOK area, Mid-Atlantic Ridge north of Kane transform, in *Tectonic, Magmatic, Hydrothermal and Biological Segmentation of Mid-Ocean Ridges*, edited by C. J. MacLeod, P. A. Tyler, and C. L. Walker, *Geol. Soc. Spec. Publ.*, 118, 61–102.
Lin, J., G. M. Purdy, H. Schouten, J.-C. Sempere, and C. Zervas (1990), Evidence from gravity data for focused magmatic accretion along the Mid-Atlantic Ridge, *Nature*, *344*, 627–632.
Lundstrom, C. C., D. E. Sampson, M. R. Perfit, J. Gill, and Q. Williams (1999), Insights into mid-ocean ridge basalt petrogenesis. U-series disequilibria from the Siqueiros Transform, Lamont Seamounts, and East Pacific Rise, *J. Geophys. Res.*, *104*, 13,035–13,048.
Magde, L. S., A. H. Barclay, D. R. Toomey, R. S. Detrick, and J. A. Collins (2000), Crustal magma plumbing within a segment of the Mid-Atlantic Ridge, 35°N, *Earth Planet. Sci. Lett.*, *175*, 55–67.
Minshull, T. A., N. J. Bruguier, and J. M. Brozena (1998), Ridge-plume interactions or mantle heterogeneity near Ascension Island?, *Geology*, *26*, 115–118.
Parson, L. M., et al. (1993), En echelon axial volcanic ridges at the Reykjanes Ridge: A life cycle of volcanism and tectonics, *Earth Planet. Sci. Lett.*, *117*, 73–87.
Passmore, E., J. Maclennan, G. Fitton, and T. Thordarson (2012), Mush disaggregation in basaltic magma chambers: Evidence from the AD 1783 Laki eruption, *J. Petrol.*, *53*, 2593–2623.
Peirce, C., A. Gardiner, and M. Sinha (2005), Temporal and spatial cyclicity of accretion at slow-spreading ridges—Evidence from the Reykjanes Ridge, *Geophys. J. Int.*, *163*, 56–78.

Perfit, M. R., and W. W. Chadwick (1998), Magmatism at Mid-ocean ridges: Constraints from volcanological and geochemical investigations, in *Faulting and Magmatism at Mid-Ocean Ridges*, edited by W. R. Buck et al., pp. 59–115, AGU, Washington, D. C.

Rossi, M. J. (1997), Morphology of the 1984 open-channel lava flow at Krafla volcano, northern Iceland, *Geomorphol.*, *20*, 95–112.

Rubin, K. H., and J. D. Macdougall (1990), Dating of neovolcanic MORB using (^{226}Ra/^{230}Th) disequilibrium, *Earth Planet. Sci. Lett.*, *101*, 313–322.

Rubin, K. H., and J. M. Sinton (2007), Inferences on mid-ocean ridge thermal and magmatic structure from MORB compositions, *Earth Planet. Sci. Lett.*, *260*, 257–276.

Rubin, K. H., I. van der Zander, M. C. Smith, and E. C. Bergmanis (2005), Minimum speed limit for ocean ridge magmatism from ^{210}Pb-^{226}Ra-^{230}Th disequilibria, *Nature*, *437*, 534–538.

Rubin, K. H., J. M. Sinton, J. MacLennan, and E. Hellebrand (2009), Magmatic filtering of mantle compositions at mid-ocean-ridge volcanoes, *Nat. Geosci.*, *2*, 321–328.

Searle, R. C., et al. (2010), Structure and development of an axial volcanic ridge: Mid-Atlantic Ridge, 45°N, *Earth Planet. Sci. Lett.*, *299*, 228–241.

Shimizu, N. (1998), The geochemistry of olivine-hosted melt inclusions in a FAMOUS basalt ALV519-4-1, *Phys. Earth Planet. Inter.*, *107*, 183–201.

Sigmarsson, O., M. Condomines, K. Grönvold, and T. Thordarson (1991), Extreme magma homogeneity in the 1783-84 Lakagigar eruption: Origin of a large volume of evolved basalt in Iceland, *Geophys. Res. Lett.*, *18*, 2229–2232.

Sims, K. W. W., et al. (2002), Chemical and isotopic constraints on the generation and transport of magma beneath the East Pacific Rise, *Geochim. Cosmochim. Acta*, *66*, 3481–3504.

Sinha, M. C., S. C. Constable, C. Peirce, A. White, G. Heinson, L. M. MacGregor, and D. A. Navin (1998), Magmatic preocesses at slow spreading ridge: Implications of the RAMESSES experiment at 57°45′N on the Mid-Atlantic Ridge, *Geophys. J. Int.*, *135*, 731–745.

Sinton, J. M., and R. S. Detrick (1992), Mid-ocean ridge magma chambers, *J. Geophys. Res.*, *97*, 197–216.

Sinton, J. M., E. C. Bergmanis, K. H. Rubin, R. Batiza, T. K. P. Gregg, K. Grönvold, K. C. Macdonald, and S. M. White (2002), Volcanic eruptions on mid-ocean ridges: New evidence from the superfast spreading East Pacific Rise, 17-19°S, *J. Geophys. Res.*, *107*(B6), doi:10.1029/2000JB000090.

Smith, D. K., and J. R. Cann (1993), Building the crust at the Mid-Atlantic Ridge, *Nature*, *365*, 707–715.

Soule, S. A., D. J. Fornari, M. R. Perfit, and K. H. Rubin (2007), New insights into mid-ocean ridge volcanic processes from the 2005-2006 eruption of the East Pacific Rise, 9°46′N-9°56′N, *Geology*, *35*, 1079–1082.

Stakes, D. S., J. W. Shervais, and C. A. Hopson (1984), The volcanic-teconic cycle of the FAMOUS and AMAR valleys, Mid-Atlantic Ridge (36°47′N): Evidence from basalt glass and phenocryst compositional variations for a steady state magma chamber beneath the valley midsections, AMAR 3, *J. Geophys. Res.*, *89*, 6995–7028.

Sturm, M. E., S. J. Goldstein, E. M. Klein, J. A. Karson, and M. T. Murrell (2000), Uranium-series age constraints on lavas from the axial valley of the Mid-Atlantic Ridge, MARK area, *Earth Planet. Sci. Lett.*, *181*, 61–70.

Thordarson, T., and G. Larsen (2007), Volcanism in Iceland in historical time: Volcano types, eruption styles and eruptive history, *J. Geody.*, *43*, 118–152.

Thordarson, T., and S. Self (1993), The Laki (Skaftar Fires) and Grimsvotn eruptions in 1783-1785, *Bull. Volcanol.*, *55*, 233–263.

Tolstoy, M., A. J. Harding, and J. A. Orcutt (1993), Crustal thickness on the Mid-Atlantic Ridge: Bull's eye gravity anomalies and focused accretion *Science*, *262*, 726–729.

Tucholke, B. E. J., J.-Q. Lin, M. C. Kleinrock, M. K. Tivey, T. B. Reed, J. Goff, and G. E. Jaroslow (1997), Segmentation and crustal structure of the western Mid-Atlantic Ridge flank, 25°25′-27°10′N and 0-29 m.y., *J. Geophys. Res.*, *102*, 10,203–10,223.

Turner, S. P., T. Kokfelt, F. Hauff, K. Haase, C. Lundstrom, K. Hoernle, I. Yeo, and C. Devey (2015), Mid-ocean ridge basalt generation along the slow-spreading, South Mid-Atlantic Ridge (5–11°S): Inferences from 238U–230Th–226Ra disequilibria, *Geochim. Cosmochim. Acta*, *169*, 152–166.

Wanless, V. D., and A. M. Shaw (2012), Lower crustal crystallization and melt evolution at mid-ocean ridges, *Nat. Geosci.*, *5*, 651–655.

Waters, C. L., K. W. W. Sims, S. A. Soule, J. Blichert-Toft, N. W. Dunbar, T. Plank, J. Prytulak, R. A. Sohn, and M. A. Tivey (2013), Recent volcanic accretion at 9°N-10°N East Pacific Rise as resolved by combined geochemical and geological observations, *Geochem.Geophys. Geosyst.*, *14*, 2547–2574, doi:10.1002/ggge.20134.